ELSEVIER

Precambrian Research 111 (2001) 165–202

Precambrian Research

www.elsevier.com/locate/precamres

Global events across the Mesoproterozoic–Neoproterozoic boundary: C and Sr isotopic evidence from Siberia

Julie K. Bartley [a,*], Mikhail A. Semikhatov [b], Alan J. Kaufman [c], Andrew H. Knoll [d], Michael C. Pope [e], Stein B. Jacobsen [f]

[a] *Department of Geosciences, State University of West Georgia, Carrollton, GA 30118, USA*
[b] *Geological Institute, Russian Academy of Sciences, Moscow 109017, Russian Federation*
[c] *Department of Geology, University of Maryland, College Park, MD 20742, USA*
[d] *Botanical Museum, Harvard University, 26 Oxford Street, Cambridge, MA 02138, USA*
[e] *Geology Department, Washington State University, Pullman, WA 99164, USA*
[f] *Earth and Planetary Sciences, Harvard University, 20 Oxford Street, Cambridge, MA 02138, USA*

Received 15 March 2000; accepted 20 June 2000

Abstract

Thick, unmetamorphosed successions of siliciclastic and carbonate rocks in eastern and western Siberia preserve a record of Middle Riphean to Early Upper Riphean sedimentary environments and geochemistry. Consistent with data from other continents, our studies in the Uchur–Maya region in southeastern Siberia and the Turukhansk Uplift in northwestern Siberia suggest a first-order shift in $\delta^{13}C$ from values near 0‰ in the early Mesoproterozoic to values near +3.5‰ after about 1300 Ma. Over this same interval, primary $^{87}Sr/^{86}Sr$ values decrease from >0.7060 to <0.7053. Combining lithologic, biostratigraphic, and geochemical data sets with available geochronologic constraints, we present a refined correlation between these two key Proterozoic successions in Siberia and add this dataset to a growing body of C and Sr isotopic data from this time interval. Carbon isotope chemostratigraphy from these regions supports the occurrence and timing of a first-order, ~3.5‰ positive shift ca. 1250–1300 Ma, approximately coeval with the onset of active margin activity that predates the main phase of Rodinia assembly. Sr isotopic data may also be interpreted within the context of the evolving Mesoproterozoic tectonic regime. Available data suggest that no dramatic rise in $^{87}Sr/^{86}Sr$ heralds the main phase of Rodinia assembly in the terminal Mesoproterozoic, suggesting that significant juvenile crust was involved in mountain building, that relative hydrothermal flux from mid-ocean ridges remained high throughout the assembly of Rodinia and/or that increased continental runoff related to intense erosion of Grenvillian mountain belts terminated shortly after orogeny.

Keywords: Proterozoic; Siberia; Chemostratigraphy; Carbonate; C-isotope; Sr-isotope

* Corresponding author. Tel.: +1-770-8302315; fax: +1-770-8364373.
E-mail address: jbartley@westga.edu (J.K. Bartley).

0301-9268/01/$ - see front matter
PII: S0301-9268(01)00160-7

1. Introduction

Secular changes in C and Sr isotopic compositions have proved useful both as correlation tools and as biogeochemical indicators in late Neoproterozoic (ca. 850–543 Ma) carbonates, permitting relatively fine-scale correlation of successions worldwide (Kaufman and Knoll, 1995; Brasier et al., 1996; Kaufman et al., 1997). Furthermore, the pronounced fluctuations in C, Sr, and S isotopic composition observed during this interval likely record similarly strong changes in climate, global C cycling and the atmospheric oxygen budget (Derry et al., 1992; Knoll, 1992; Des Marais, 1994; Strauss, 1997; Hoffman et al., 1998; Canfield, 1999).

In contrast to the late Neoproterozoic, earlier Proterozoic isotopic variations are less well constrained. Available data indicate that late Paleoproterozoic to early Mesoproterozoic ($> \sim 1300$ Ma) successions have average $\delta^{13}C$ values near $0 \pm 1‰$, with stratigraphic variations of no more than a few permil (Pokrovsky and Vinogradov, 1991; Buick et al., 1995; Knoll et al., 1995; Khabarov et al., 1996; Frank et al., 1997; Xiao et al., 1997; Brasier and Lindsay, 1998). Based on such datasets, the Mesoproterozoic has been cited as a time of biogeochemical stasis (Buick et al., 1995; Brasier and Lindsay, 1998; Knoll and Canfield, 1998). In apparent contrast, the end of the Mesoproterozoic Era has long been recognized as a time of tectonic upheaval resulting in the assembly of a supercontinent (McMenamin and McMenamin, 1990; Hoffman, 1991; Powell et al., 1993), as well as an interval of significant evolutionary innovation and diversification among eukaryotic groups (Butterfield et al., 1990; Knoll and Sergeev, 1995; Xiao et al., 1997; Butterfield, 2001). The end of the Mesoproterozoic Era may also be marked by a change in atmospheric oxygen content (Des Marais et al., 1992; Canfield, 1999).

Indeed, recent studies indicate that late Mesoproterozoic to early Neoproterozoic successions (ca. 1300–850 Ma) exhibit moderately positive average $\delta^{13}C$ values, with $\delta^{13}C$ oscillations between about $-2‰$ and $+4‰$ (Fairchild et al., 1990; Knoll et al., 1995; Podkovyrov and Vinogradov, 1996; Podkovyrov et al., 1998; Kah et al., 1999), with short intervals of strongly positive $\delta^{13}C$ values (up to $+5–6‰$), recognized only locally in uppermost Mesoproterozoic sections (Podkovyrov and Vinogradov, 1996; Vinogradov et al., 1998). By late Neoproterozoic standards, these secular variations are small; however, the evolution of $\delta^{13}C$ from an average of $\sim 0‰$ to $\sim +3‰$ marks a significant change in the biogeochemical cycling of carbon. Thick, exceptionally well preserved carbonate successions of Siberia record biological and geochemical changes across the chronometric (1000 Ma) Mesoproterozoic–Neoproterozoic boundary (approximately, but not precisely equivalent to the chronostratigraphic Middle–Upper Riphean boundary), potentially providing critical information about late Mesoproterozoic seawater composition and concomitant global tectonic and biogeochemical changes.

The dynamics of the global C cycle are closely linked with global tectonics; for example, high sedimentation rates during periods of mountain building are believed to be associated with high proportional rates of organic C burial (Raymo et al., 1988; Berner and Canfield, 1989; Derry et al., 1992; Kaufman et al., 1993; Des Marais, 1994, 1997a,b). Thus, an interpretation of C cycle stasis (Brasier and Lindsay, 1998) is potentially at odds with geologic evidence for significant continental assembly during the late Mesoproterozoic (Grenvillian events, i.e. Elzevirian and Ottawan orogenies; ca. 1300–1070 Ma, McLelland et al., 1996). Because radiogenic Sr is typically introduced to the ocean during uplift and erosion of ancient continental crust, seawater $^{87}Sr/^{86}Sr$ in the latter half of the Mesoproterozoic would be predicted to rise, reflecting increased crustal erosion of older granitic crust during Grenvillian events. On the other hand, if these orogenies exposed relatively young crust, the $^{87}Sr/^{86}Sr$ of seawater could conceivably stay the same, or even fall, depending on the flux and isotopic composition of eroding material. To date, poor temporal resolution has prevented detailed evaluation of secular change in seawater $^{87}Sr/^{86}Sr$ through the Mesoproterozoic Era. At present, the few analyses available for $^{87}Sr/^{86}Sr$ of well-preserved carbonates suggest that Mesoproterozoic seawater was

dominated by non-radiogenic sources (Pokrovsky and Vinogradov, 1991; Mirota and Veizer, 1994; Gorokhov et al., 1995; Hall and Veizer, 1996; Kah et al., 2001).

The transition from a characteristically early Mesoproterozoic record of little $\delta^{13}C$ change to the moderate variability noted in the late Mesoproterozoic has not been documented within any single succession, nor have the postulated changes in $^{87}Sr/^{86}Sr$ (Mirota and Veizer, 1994; Gorokhov et al., 1995). The Turukhansk and Uchur–Maya regions of Siberia thus have the potential to address questions of changing seawater chemistry through this critical interval. The studied parts of these successions span the Middle to Upper Riphean transition, and contain carbonates that retain little-altered C and Sr isotopic signatures. By considering C and Sr isotopic data from the two regions in combination with regional stratigraphy, paleontology, and paleomagnetic data, we propose a refined correlation between these widely separated, key Riphean successions of the Siberian craton. Correlation between these two basins permits refinement of isotopic curves during the assembly of Rodinia.

2. Geologic setting and regional correlations – Turukhansk and Uchur–Maya regions

Riphean sedimentary rocks are exposed along both the eastern and western margins of the Siberian craton, in the Uchur–Maya and Turukhansk regions (Figs. 1 and 2). These thick successions of carbonates and siliciclastics represent intervals of broadly contemporaneous deposition in the shallow marine platforms surrounding Siberia during the Proterozoic. Lithologic, biostratigraphic, geochronologic, and paleomagnetic evidence suggest close correlation between these regions, although detailed correlation is somewhat complicated by a relative paucity of reliable geochronologic data.

2.1. The Turukhansk region

The Turukhansk region is an uplifted margin along the northwestern edge of the Siberian Cra-ton. Within the uplift, unmetamorphosed

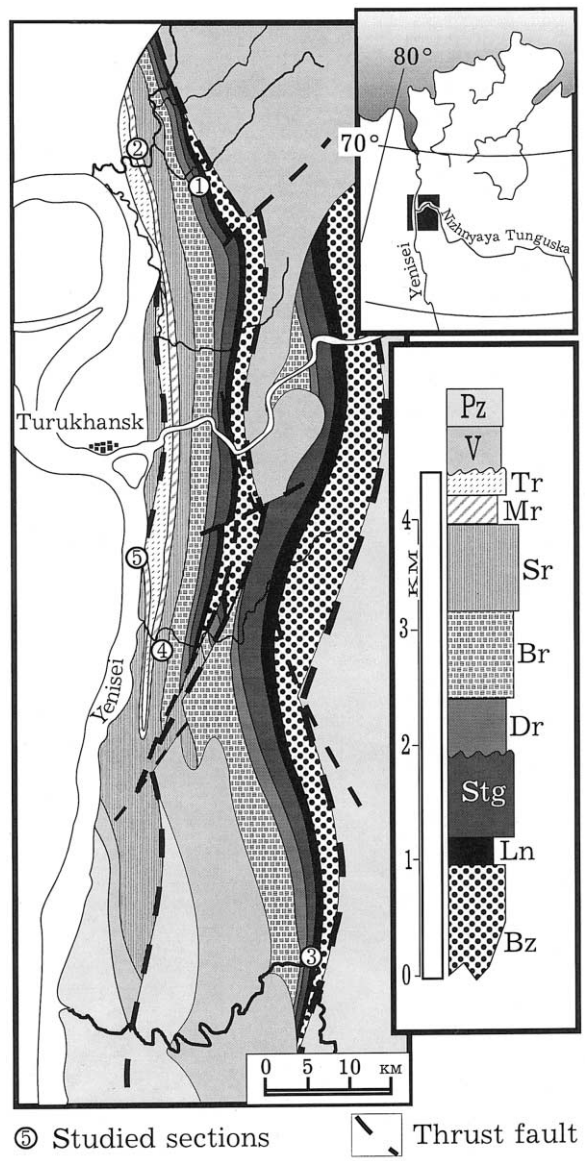

Fig. 1. Geologic map of the Turukhansk region, showing locations of the studied sections. Geologic units are as follows. Bz – Bezymyannyi Formation, Ln – Linok Formation, Stg – Sukhaya Tunguska Formation, Dr – Derevnya Formation, Br – Burovaya Formation, Sr – Shorikha Formation, Mr – Miroyedikha Formation, Tr – Turukhansk Formation, V – Vendian deposits, Pz – Paleozoic deposits. Numbers 1–5 correspond to sections examined in this study. 1 – Kammennaya River, 2 – Bol'shaya Shorikha River, 3 – Sukhaya Tunguska River, 4 – Miroyedikha River, 5 – Yenisei River. Map compiled by P.Yu. Petrov.

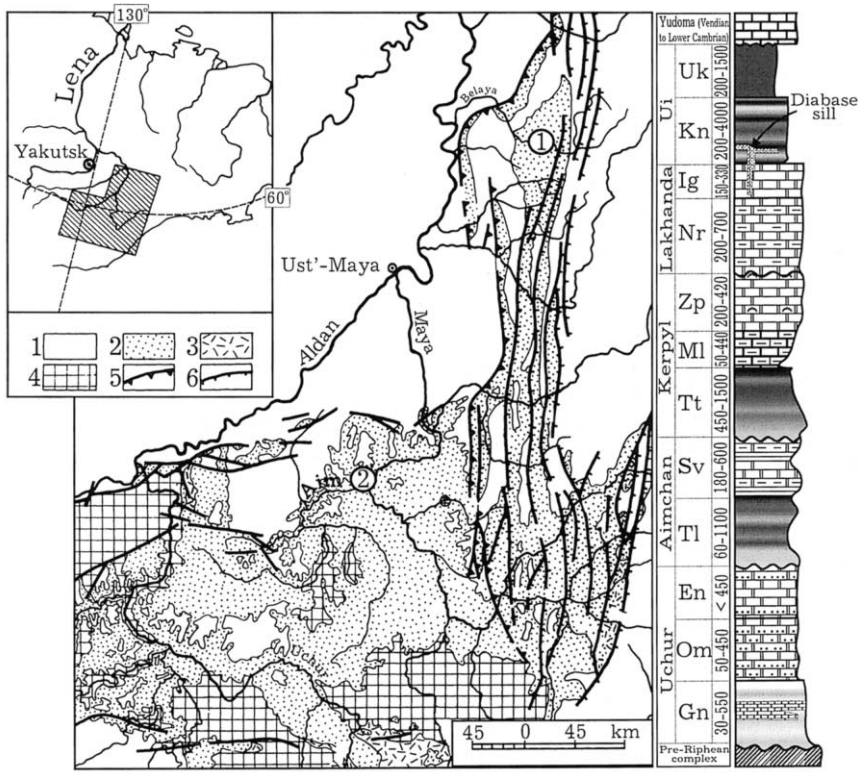

Fig. 2. Geological sketch map of the Uchur–Maya region showing locations of the studied sections. Geologic units abbreviated on the stratigraphic column are as follows. Gn – Gonam Formation, Om – Omachta Formation, En – Ennina Formation, Tl – Talyn Formation, Sv – Svetlyi Formation, Tt – Totta Formation, Ml – Malgina Formation, Zp – Tsipanda Formation, Nr – Neryuen Formation, Ig – Ignikan Formation, Kn – Kandyk Formation, Uk – Ust'-Kirba Formation. Legend to geologic units: 1 – Phanerozoic deposits, 2 – Vendian and Riphean deposits, 3 – Late Paleoproterozoic volcano-plutonic complex, 4 – Archean and Early Paleoproterozoic crystalline basement, 5 – major thrust fault delimitating the Uchur–Maya Plate on the south-west and the Uchur–Maya Belt on the east, 6 – thrust fault within the Yudoma–Maya Belt. Circled numbers on the map correspond to studied sections: 1 – Belaya River and Svetlyi Creek, 2 – Exposures near the confluence of the Aim and Maya Rivers (Semikhatov and Serebryakov, 1983).

Riphean carbonates and siliciclastic rocks, up to 4.5 km thick, are exposed in three north–south trending, east-transported, thrust-bounded blocks (Fig. 1; Semikhatov and Serebryakov, 1983; Petrov and Semikhatov, 1997, 1998). In the western and eastern blocks, sedimentary deposits form gently dipping (15–30°), westward deepening homoclines, complicated by small faults. Sediments of the central block form an asymmetrical syncline with a subvertical, truncated western limb, also complicated by small faults. A regional erosional surface separates the Riphean sediments of the Turukhansk region into two packages: a lower, Middle Riphean succession, and an upper, Upper Riphean succession. The lower package commences with the siliciclastic Bezymyannyi Formation which accumulated within an open marine basin near storm wave base (Petrov, 1993b; Veis and Petrov, 1994). Conformably overlying the Bezymyannyi the predominantly carbonate Linok Formation (180–380 m thick) was deposited below and near storm wave base along an extensive carbonate platform, which shoals near the top of the formation (Petrov, 1993a; Veis and Petrov, 1994). Limestones and dolostones of the Sukhaya Tunguska Formation (560–680 m) accumulated in upper subtidal to intertidal settings (Petrov et al., 1995; Sergeev et al., 1997; Sergeev, 1999).

Above the erosional surface, the upper succession commences with the dolomites and shales of Derevnya Formation (75–270 m), accumulated in a shelf setting (Petrov and Veis, 1995). Carbonates of this formation contain spectacular *Jacutophyton* cycles (Serebryakov, 1975, 1976) and shales preserve a diverse acritach assemblage (Petrov and Veis, 1995). Conformably overlying the Derevnya Formation, the Burovaya Formation (350–1000 m) records development of a carbonate ramp and associated stromatolitic reef (Petrov and Semikhatov, 1998, 2001). Burovaya carbonates are disconformably overlain by peritidal to shallow marine dolostones of the Shorikha Formation (500–1000 m; Sergeev et al., 1997), the mixed siliciclastic-carbonate Miroyedikha Formation, dominated by open shelf environments (150–250 m; Petrov and Semikhatov, 1997), and the dolomitic Turukhansk Formation, accumulated on an open shelf below fair weather wave base (Petrov and Semikhatov, 1997).

2.1.1. Radiometric determinations

Radiometric data from the Turukhansk Riphean succession are limited, but broadly constrain the age of deposition. A 16-point Pb–Pb isochron on carbonates from the middle Sukhaya Tunguska Formation yielded an age of 1035 ± 60 Ma (Ovchinnikova et al., 1995). K–Ar determinations on globular glauconite from the Bezymyannyi (830–910 Ma), Derevnya (800–860 Ma), and Burovaya (830–895 Ma) Formations reflect resetting of the K–Ar clock 850–900 Ma (Semikhatov and Serebryakov, 1983; Gorokhov et al., 1995 and references therein). Units correlative to the Turukhansk Riphean succession on the Yenisei Ridge are cut by ca. 830 Ma granites (Shenfil', 1991 and references therein).

2.1.2. Biostratigraphy

Organic-walled microfossils occur in shales of the Bezymyannyi, Derevnya and Miroyedikha Formations, and suggest that the Middle–Upper Riphean boundary be placed at the erosional unconformity separating the Sukhaya Tunguska and Derevnya Formations. The Bezymyannyi assemblage contains mostly simple and long-ranging acritarch and cyanobacteria-like microfossils, as well as broad thalli with longitudinal striations and rare acanthomorphic acritarchs (*Trachyhystrichosphaera parva* Mikhailova). Based on the size and relatively complex morphology of these fossils, Veis (1988) and Veis and Petrov (1994) assigned the Bezymayannyi Formation to the Upper Riphean. However, occurrences of the same morphotypes in shales underlying the type Riphean succession in the Urals (Veis et al., 2000) and in the 1480–1450 Ma (Gorokhov et al., 1997) Ust'Il'ya and Kotuikan shales of the Anabar Massif (Veis and Vorob'eva, 1992), as well as comparison with other Middle–Lower Riphean biotas (Sergeev et al., 1995) indicates that the Bezymyannyi assemblage of microfossils is consistent with the Middle Riphean age. In contrast, Derevnya shales contain a diverse acritarch assemblage that includes several characteristic Upper Riphean taxa, including the three distinctive acanthomorphic acritarchs *Trachyhystrichosphaera aimica* German [= Hermann], *T. stricta* German, and *T. truncata* German et Jankauskas. Shales of the Miroyedikha Formation contains a well-preserved microfossil assemblage that includes diverse, morphologically complex acritarchs and algae, consistent with an Upper Riphean age (German, 1981a,b; Hermann [= German], 1990; Veis et al., 1998a, 1999).

The above age constraints, based on organic-walled microfossils, are consistent with the succession of stromatolite assemblages, which were originally used to define the Middle–Upper Riphean boundary in the Turukhansk succession (Semikhatov, 1962; Semikhatov and Serebryakov, 1983; Shenfil', 1991, and references therein). The Derevnya and Burovaya Formations contain an assemblage of distinctive Lower–Upper Riphean morphotypes superimposed on the background of endemic transitional Middle–Upper Riphean taxa that occur in the older units of the succession.

2.2. The Uchur–Maya region

The Uchur–Maya region (Fig. 2) comprises nearly 100 000 km^2 of exposed Riphean sediments that rest unconformably on Archean and Late

Paleoproterozoic rocks, and unconformably underlie Vendian (Yudomian) through Middle Cambrian sediments. Two distinctive tectonic structures, separated by an eastward-dipping thrust, are located within the region: the Uchur–Maya Plate in the southwest and the north–south trending Yudoma–Maya Belt in the east (Nuzhnov and Yarmolyuk, 1959; Semikhatov and Serebryakov, 1983). Within the Uchur–Maya Plate, Riphean to Middle Cambrian deposits lie subhorizontally and record deposition in epicratonic basins developed along the eastern edge of the Siberian Platform. The Yudoma–Maya Belt forms open asymmetrical folds complicated by a number of strike-slip and west-directed thrust-faults. Deposition of Middle Riphean through Vendian sediments occurred in a rift-related trough.

The Riphean succession in the Uchur–Maya region is subdivided into five unconformity-bounded groups, which are described in detail in previous publications (Komar et al., 1978; Semikhatov and Serebryakov, 1978, 1983; Shenfil', 1991). Of interest in this study are the upper four groups: the Aimchan, Kerpyl', Lakhanda and Ui, which are Middle to Late Riphean in age.

The Middle Riphean Aimchan Group rests with angular unconformity on the Lower Riphean sediments of the Uchur Group, or on Archean crystalline basement (Semikhatov and Serebryakov, 1983, Fig. 42). It is exposed in the Yudoma–Maya Belt and along the eastern edge of the Uchur–Maya Plate. The peritidal siliciclastic sediments of the Talyn Formation comprise the lower part of the Aimchan Group, and the predominantly subtidal Svetlyi Formation, containing carbonates and subordinate shales, constitutes the upper part of the group.

The Kerpyl' Group rests unconformably on older rocks (Semikhatov and Serebryakov, 1983, Fig. 43) and is composed of the mainly siliciclastic Totta Formation, limestones of the Malgina Formation, and dolostones of the Tsipanda Formation. Contacts within the Kerpyl' Group are conformable, and the Malgina–Tsipanda boundary may be time-transgressive (Semikhatov and Serebryakov, 1983).

The overlying Lakhanda Group is separated from Tsipanda dolostones by an ancient weathered surface containing both bauxite and kaolinite in the Uchur–Maya Plate sections but rests with apparent conformity on the upper Tsipanda Formation within the Yudoma–Maya Belt. The Neryuen Formation (220–340 m) comprises the lower part of the group, and consists mainly of shale, siltstone, limestone and dolostone. Carbonates of the Neryuen Formation are frequently stromatolitic, and the middle part of the Neryuen contains prominent *Jacutophyton* cycles (Serebryakov, 1975, 1976). Shales of western exposures of the Neryuen Formation contain superbly preserved microfossils (Hermann, 1990; Veis et al., 1998a,b). The Ignikan Formation (130–380 m) comprises the upper Lakhanda Group and is dominated limestones and dolostones accumulated in upper subtidal environments. The overlying siliciclastic Ui Group is the uppermost Riphean unit in the region and in most sections rests conformably on the Ignikan carbonates. Complete sections of the Ui Group occur only in eastern exposures, within the Yudoma–Maya Belt. Elsewhere, the group is truncated by the pre-Vendian unconformity and pinches out along the eastern margin of the Uchur–Maya Plate. Preserved thicknesses of the Ui Group vary greatly, ranging from 400–550 m in Uchur–Maya Plate sections to 3.3–3.5 km in the Yudoma–Maya Belt.

2.2.1. Radiometric determinations

The maximum age of the Riphean succession in the Uchur–Maya region is constrained by U–Pb determinations of 1703 ± 18, 1727 ± 11 and 1727 ± 6 Ma (Neymark et al., 1992; Nutman et al., 1992; Larin et al., 1997) on zircon and monazite from the youngest members of the pre-Uchur Group volcano-plutonic complex. Numerous isotopic age determinations on glauconite-illite series minerals for the Uchur Group (1500–1360 Ma), the Aimchan Group (1260–1200 Ma), Kerpyl' Group (1170–860 Ma), and Lakhanda Group (970–870 Ma) all fit the expected stratigraphic trend for age dates (see Semikhatov and Serebryakov (1983), Shenfil' (1991), and references therein). These data have been traditionally interpreted to record depositional ages. However, several of these data appear to be at odds with recent

U–Pb analyses on baddelyite from mafic sills that cut the Lakhanda and lower Ui Groups, and are dated at 974 ± 18 and 1004 ± 5 Ma (Rainbird et al., 1998). A Sm–Nd isochron age of the same sills yielded an age of 948 ± 18 Ma (Pavlov et al., 1992). A Pb–Pb isochron of carbonates from the lower Lakhanda Group yielded an age of 1025 ± 40 Ma (Semikhatov et al., 2000). These new constraints suggest that the Upper Riphean Lakhanda Group is Mesoproterozoic in age. A maximum age for the Kerpyl' Group is provided by U–Pb dating of detrital zircons in the Totta Formation (Khudoley et al., in press); the youngest population yielded an age of 1300 ± 5 Ma. Thus, the studied succession in the Uchur–Maya region spans much of the latter part of the chronometrically defined Mesoproterozoic Era.

2.2.2. Biostratigraphy

Organic-walled microfossils from the Riphean of the Uchur–Maya region display a stratigraphic pattern similar to that seen in the Turukhansk region (Pyatiletov, 1988; Veis, 1988; Veis and Semikhatov, 1989; Hermann, 1990; Petrov and Veis, 1995; Veis et al., 1998b). The earliest assemblage, in the Uchur Group, consists of long-ranging, stratigraphically uninformative taxa, including small, simple acritarchs, simple colonial coccoids, and filaments. Kerpyl' shales, in turn, preserve a microfossil assemblage much like that of the Bezymyannyi Formation in the Turukhansk region. Neryuen shales, in the lower Lakhanda Group, are marked by the appearance of a number of morphotypes, including acanthomorphic acritarchs (*Trachyhystrichosphaera aimica* Hermann and *T. stricta* Hermann), large ellipsoidal vesicles (*Lakhandinia*), algal thalli (*Plicatidium*, *Archeoclada* and *Veleriaclada*), and complex problematica (*Mucorites*, *Majasphaeridium*, *Eosaccharomyces*; Pyatiletov, 1988; Veis, 1988; Jankauskas et al., 1989; Hermann, 1990; Veis et al., 1998b, 2000). The genus *Paleovaucheria*, originally described from Neryuen shales, has been confirmed as a xanthophyte alga (Woods et al., 1998). The Neryuen assemblage is thus similar to both the Derevnya microfossil assemblage and to microbiotas in shales of the lower part of the Upper Riphean stratotype (Ural Mountains) and its cis-Uralian analogues (Keller, 1982; Jankauskas et al., 1989; Veis et al., 1998b, 2000). The changes in taxonomic composition of organic-walled microfossils at the base of the Lakhanda Group indicate that the Middle–Upper Riphean boundary should be placed between the Kerpyl' and Lakhanda Groups in the Uchur–Maya region. The Ui Group microbiota is similar to that of the Lakhanda Group, but is less diverse; however, it contains a number of new taxa, including the distinctive acritarchs *Cymatiosphaera* and *Granomarginata* (Volkova, 1981; Pyatiletov, 1988; Jankauskas et al., 1989). In the Uchur–Maya region, as in the Turukhansk Uplift, the biostratigraphic ages suggested by organic-walled microfossils are consistent with the observed succession of stromatolite taxa (Nuzhnov and Yarmolyuk, 1959; Semikhatov and Serebryakov, 1983; Shenfil', 1991), which supports the conclusion that the Middle–Upper Riphean boundary occurs at the base of the Laskhanda Group.

2.3. Correlations between the Turukhansk and Uchur–Maya regions

Correlations of Riphean sediments of western (Turukhansk Uplift and Yenesei Ridge) and eastern (Uchur–Maya region) Siberia (Fig. 3) were based on a striking coincidence in superposition of lithologies (Semikhatov and Serebryakov, 1983), on a compositional resemblance of successive stromatolite assemblages (Semikhatov, 1962; Semikhatov and Serebryakov, 1983; Semikhatov, 1991; Shenfil', 1991), on similarities in microfossil assemblages (German, 1981a,b; Pyatiletov, 1988; Veis, 1988; Jankauskas et al., 1989; Hermann, 1990; Veis et al., 1998a,b, 1999), on paleomagnetic data (Pavlov and Petrov, 1996; Gallet et al., 2000) and on radiometric age data (see Semikhatov and Serebryakov (1983) and Shenfil' (1991) for bibliography and review).

The biostratigraphically defined Middle–Upper Riphean boundary is placed at a distinctive regional erosional unconformity in both succession. In the Turukhansk Uplift, this unconformity separates the Sukhaya Tunguska Formation from the Derevnya Formation, and in the Uchur–Maya

region, it separates the Tsipanda Formation (Kerpyl' Group) from the Neryuen Formation (Lakhanda Group).

Late Middle Riphean sediments of both regions share a striking lithologic similarity: the succession of the siliciclastic Bezymyannyi Formation, calcitic Linok Formation and limestone–dolostone Sukhaya Tunguska Formation is a counterpart to the Totta, Malgina and Tsipanda Formations of the Kerpyl' Group. Micropaleontological studies indicate that the Totta and Bezymyannyi assemblages of organic-walled forms are nearly identical in composition (Pyatiletov, 1988; Veis, 1988; Hermann, 1990; Veis et al., 1998b). Furthermore, recent paleomagnetic data from the Uchur–Maya and Turukhansk regions (Pavlov and Petrov, 1996; Gallet et al., 2000) reveal two important features that suggest a close linkage between the Linok and Malgina Formations. First, the paleopole positions of the Linok and Malgina Formations are nearly identical, after correcting for relative motion within the Siberian craton during the Paleozoic opening of the Vilyui rift (Pavlov and Petrov, 1996; Smethurst et al., 1998). Second, both the Malgina and Linok Formations demonstrate regionally persistent and similar polarity reversals. The lower parts of both units exhibit frequent alternation of normal and reversed polarity zones, and the upper parts demonstrate a gradual disappearance of normal zones, more evident in the Linok Formation; its upper part is almost completely dominated by reversed polarity (Gallet et al., 2000). Though available data are insufficient to provide a detailed correlation between the two regions, results are consistent with correlation between the Linok and Malgina Formations.

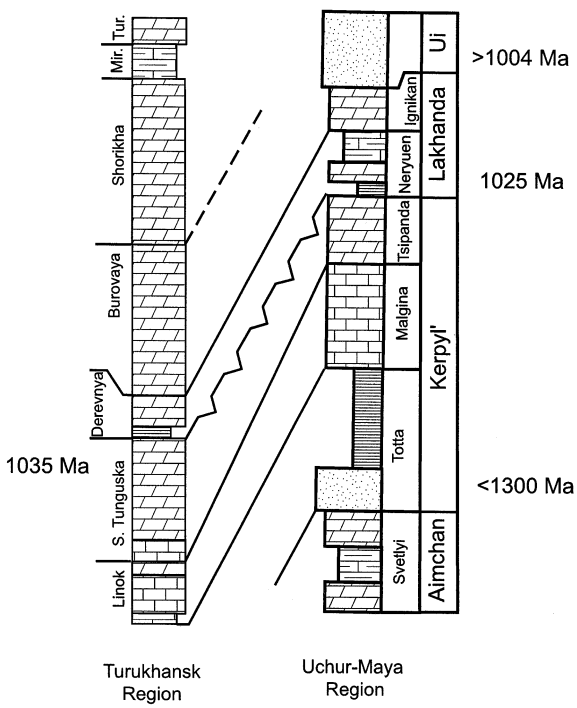

Fig. 3. Correlation between Riphean sediments of the Uchur–Maya and Turukhansk regions, based on available lithostratigraphic, geochronologic, and biostratigraphic data (Semikhatov and Serebryakov, 1983; Shenfil', 1991 and references therein). Absolute age dates are based on recent U–Pb and Pb–Pb geochronology. (1) Sukhaya Tunguska Formation, 1035 ± 60 Ma, $Pb–Pb_{carbonate}$ (Ovchinnikova et al., 1995); (2) Kerpyl Group, younger than 1300 Ma, based on U–Pb analysis of detrital zircons in the Totta Formation (Khudoley et al., in press); (3) Lower Lakhanda Group, 1025 ± 40 Ma (Semikhatov et al., 2000); Lower Ui Group, older than 1004 ± 5 Ma, based on $U–Pb_{baddelyite}$ ages (Rainbird et al., 1998).

Above the Middle–Upper Riphean disconformity, sediments of the Turukhansk and Uchur–Maya region share several similar features. The Derevnya and Neryuen Formations are characterized by distinctive cycles of the stromatolite forms *Conophyton*, *Jacutophyton* and *Baicalia*, likely produced by sea level oscillation (Bertrand-Sarfati and Moussine-Pouchkine, 1985; Petrov and Veis, 1995). Distinctive stromatolitic forms appear in the Derevnya and Neryuen Formations, including the diagnostic *Baicalia lacera* Semikhatov, *Inzeria tjomusi* Krylov and *Jurusania cylindrica* Krylov, known from Lower–Upper Riphean sediments worldwide. The characteristic microstructure of *B. lacera* occurs in a number of other Early Upper Riphean stromatolite morphotypes in northern Eurasia, northern Africa, and North America and likely documents a particular stage in the secular global changes in early carbonate cementation and diagenesis (Knoll and Semikhatov, 1998). The Middle Riphean parts of both successions contain endemic and long-ranging Middle–Upper Riphean stromatolites. The well-preserved, diverse microfossil assemblages of the Derevnya and Neryuen Formations are strikingly similar, and

likely preserve flora of similar age (Pyatiletov, 1988; Veis, 1988; Hermann, 1990; Veis et al., 1998b).

Taken together, available biostratigraphic, sedimentological, paleomagnetic, and lithostratigraphic data suggest the broad correlation depicted in Fig. 3. In the present study, we attempt to use chemostratigraphic data, in conjunction with the lines of evidence outlined above to refine correlations between eastern and western Siberia and to place these successions within an emerging global framework of secular trends in Proterozoic seawater chemistry.

3. Constraining the Middle–Upper Riphean boundary

Although microfossil evidence clearly suggests that the Middle–Upper Riphean boundary should be located at the unconformity between the Sukhaya Tunguska and Derevnya Formations in the Turukhansk Uplift and between the Tsipanda and Neryuen Formations in the Uchur–Maya region, the radiometric age of the boundary remains poorly constrained in the current Russian Precambrian chronostratigraphic scale, as does its relationship to the Mesoproterozoic–Neoproterozoic boundary. The Middle–Upper Riphean boundary is generally considered to be 1000 ± 50 Ma (Semikhatov et al., 1991; Semikhatov, 1995), and thus approximately coeval with the Mesoproterozoic–Neoproterozoic boundary. Recent U–Pb age determinations on the sills that cut the Lakhanda and Ui Groups (Rainbird et al., 1998), however, indicate that this boundary is older than 1004 ± 5 Ma. A recently obtained 8-point Pb–Pb isochron on little-altered lower Lakhanda Group carbonates yields an age of 1025 ± 40 Ma (Semikhatov et al., 2000). In the Turukhansk region, Middle Riphean carbonates of the Sukhaya Tunguska Formation yield a Pb–Pb isochron age of 1035 ± 60 Ma (Ovchinnikova et al., 1995). Within analytical error, these data indicate that the radiometric age of the Middle–Upper Riphean boundary is ca. 1030 Ma, suggesting, therefore, that this chronostratigraphically defined boundary (Semikhatov et al., 1991; Semikhatov, 1995) may predate the chronometrically defined Mesoproterozoic–Neoproterozoic boundary (Plumb, 1990) by a few tens of millions of years (also see discussion in Xiao et al. (1997)).

4. Methods

4.1. Field sampling

Three sample sets were collected from the Turukhansk region for Sr and C isotopic analysis during a joint US–Russian expedition in 1995. The first was obtained in the central fault-bounded block along the Kammennaya and Bol'shaya Shorikha Rivers in the northern part of the region (Fig. 1, Sections 1 and 2). Limestones were collected from the Linok, Sukhaya Tunguska, and Burovaya Formations (Samples K95-6–K95-43; Table 1), and dolostones from the Miroyedikha Formation (Samples K95-51–K95-50; Table 1). The second suite (Fig. 1, Sections 4 and 5) represents sampling of the Shorikha, Miroyedikha, and Turukhansk Formations, exposed in the same block along the Miroyedikha and Yenisei Rivers (Samples beginning K95-129-, K95-139-, K95-140- and K95-142-; Table 1). The third sample set was collected in the Sukhaya Tunguska Formation in the eastern block (Fig. 1, Section 3), along the Sukhaya Tunguska River, in the southern part of the region (Samples K95-72–K95-95; Table 1). The first two sets supplement material collected previously (MAS and colleagues) and explored in previous Sr isotopic (Gorokhov et al., 1995) and C isotopic (Knoll et al., 1995) studies. These new samples significantly improve the chemostratigraphic resolution of the earlier datasets. The third sample set comes from sections of correlative units along the Sukhaya Tunguska River in the southern part of the region that have not been previously sampled for chemostratigraphy.

Two sample sets were obtained from the Uchur–Maya region. The first one was collected in the northern part of the Yudoma–Maya Belt (Fig. 2, Section 1). Samples were collected from the Svetlyi Formation exposed along Svetlyi Creek, the left tributary of the Belaya River (Samples UM8–UM23), and from the Malgina For-

Table 1
Geochemical data for new analyses of samples from the Turukhansk region

Sample	Formation	Section	Height	Lithology	$\delta^{13}C$	$\delta^{13}C_{altered}$	$\delta^{18}O$	Mn (ppm)	Sr (ppm)	Sr (ID)	Fe (ppm)	Mg/Ca	Ca/Sr	Mn/Sr	Fe/Sr	Rb/Sr	$^{87}Sr/^{86}Sr$
T-30	Linok	CNTS	‘115	ls	−0.6		−8.3					0.00		0.69			0.70627
T-31	Linok	CNTS	146	ls	−0.3		−7.8					0.01		0.83			0.70611
T-33	Linok	CNTS	180	ls	0.0		−8.1					0.05		0.81			0.70652
K95-9	Linok	KAM	35.5	ls	−0.1		−9.6	238	174	1197	4647	0.01	1215	1.37	27	0.0017	0.70659
K95-10	Linok	KAM	47.5	ls	−0.1		−9.0	89	77	476	1984	0.01	1794	1.15	26	0.0120	
K95-11	Linok	KAM	56	ls	−1.9		−8.8	172	98	161	3151	0.01	2312	1.76	32	0.0077	0.70924
K95-12	Linok	KAM	66	ls	−1.1		−8.5	91	92	221	2756	0.01	2546	0.99	30	0.0047	0.70825
K95-13	Linok	KAM	76	ls	−1.0		−8.6	85	106	182	2774	0.00	2205	0.80	26	0.0047	
K95-15	Linok	KAM	86	ls	−0.4		−8.1	79	107		2739	0.01	2171	0.74	26		
K95-21	S. Tung.	KAM	271	ls		0.9	−7.1	699	45	88	1879	0.51	3233	15.46	42	0.0008	
K95-22	S. Tung.	KAM	280	ls	0.3		−7.5	24	393	472	2619	0.03	695	0.06	7	0.0005	0.70590
K95-72	S. Tung.	ST	281	ls	1.2		−7.1	25	469		3150	0.01	641	0.05	7		
K95-73	S. Tung.	ST	291	ls	1.9		−6.9	28	277	428	2501	0.00	984	0.10	9	0.0003	0.70610
K95-74	S. Tung.	ST	300	ls	1.6		−7.2	28	608		2334	0.01	439	0.05	4		
K95-75	S. Tung.	ST	311	ls	1.0		−7.1	35	494		2862	0.01	555	0.07	6		
K95-76	S. Tung.	ST	321	ls	0.2		−6.4	52	472	547	2741	0.06	524	0.11	6	0.0009	0.70588
K95-77	S. Tung.	ST	331	ls	1.3		−5.9	25	610		2837	0.03	481	0.04	5		
K95-78	S. Tung.	ST	332	ls	1.2		−6.7	19	494		2178	0.02	484	0.04	4		
K95-79	S. Tung.	ST	332	ls	1.5		−6.6	17	388	687	3107	0.01	680	0.05	8	0.0000	0.70611
K95-80	S. Tung.	ST	342	ls	2.3		−6.7	20	802		2694	0.01	370	0.03	3		
K95-81	S. Tung.	ST	351	ls	1.9		−6.2	17	517		2425	0.06	561	0.03	5		
K95-82	S. Tung.	ST	357	ls		0.2	−10.6										
K95-82B	S. Tung.	ST	357	ls	1.5		−6.5	14	264		1625	0.05	505	0.05	6		
K95-83	S. Tung.	ST	361	ls	1.1		−6.8	18	427		2457	0.04	615	0.04	6	0.0001	
K95-84	S. Tung.	ST	371	ls	2.4		−7.1	13	436		2295	0.02	568	0.03	5		
K95-84A	S. Tung.	ST	371	ls	2.4		−7.0										
K95-85	S. Tung.	ST	381	ls	1.7		−7.1	9	545		2697	0.00	540	0.02	5		
K95-86	S. Tung.	ST	391	ls	3.2		−7.1			918						0.0000	0.70571
K95-87	S. Tung.	ST	401	ls	2.6		−7.0										
K95-88-1	S. Tung.	ST	413	ls	1.1		−7.0	27	255		2807	0.02	1112	0.10	11		
K95-88-2	S. Tung.	ST	413	ls	1.2		−7.0	14	280	396	2508	0.02	973	0.05	9	0.0006	0.70567
K95-90	S. Tung.	ST	429	ls	3.3		−7.1	14	335		2639	0.01	803	0.04	8		
K95-95	S. Tung.	ST	450	ls	1.4		−7.7	22	250	312	2580	0.02	963	0.09	10	0.0027	0.70613
T-35	S. Tung.	CNTS	231	ls	2.0		−7.1					0.09		0.07			0.70560
T-37	S. Tung.	CNTS	387	ls	3.0		−8.9					0.03		0.05			0.70567
T-38	S. Tung.	CNTS	441	ls	2.3		−9.8					0.01		0.09			0.70585
T-39	S. Tung.	CNTS	474	ls	1.1		−9.2					0.01		0.19			0.70581
T-52	Derevnya	CNTS	1064	ls	1.0		−9.0					0.02		4.04			0.70614
T-64	Burovaya	CNTS	1897	ls	3.1		−6.4					0.01		0.04			0.70525
T-66	Burovaya	CNTS	2113	ls	0.3		−8.2					0.02		2.27			0.70599
T-67	Burovaya	CNTS	2159	ds	1.8		−8.9					0.52		4.80			
K95-38	Burovaya	KAM	997	ls	2.4		−5.9			158						0.0025	0.70641
K95-39	Burovaya	KAM	1022	ls	2.6		−6.1	53	226	356	2617	0.02	1263	0.23	12	0.0009	0.70555
K95-129/T-4	Shorikha	MIR	−4	ds	1.4		−4.5	53	23		1759	0.59	4717	2.31	77		
K95-129/T-2	Shorikha	MIR	−2	ds	1.3		−4.4	73	36		2376	0.56	3533	2.02	66		
K95-129/T-1	Shorikha	MIR	−1	ds	1.3		−4.1	104	27		2732	0.61	4292	3.89	103		
K95-129/T	Shorikha	MIR	0	ds	1.6		−4.5	211	31		3977	0.63	4637	6.79	128		
K95-140/T-4	Shorikha	YEN	−4	ds	0.6		−6.4	171	37		3711	0.55	4282	4.61	100		
K95-140/T-2	Shorikha	YEN	−2	ds				236	47		2795	0.42	3794	5.07	60		

Table 1 (*Continued*)

Sample	Formation	Section	Height	Lithology	$\delta^{13}C$	$\delta^{13}C_{altered}$	$\delta^{18}O$	Mn (ppm)	Sr (ppm)	Sr (ID)	Fe (ppm)	Mg/Ca	Ca/Sr	Mn/Sr	Fe/Sr	Rb/Sr	$^{87}Sr/^{86}Sr$
K95-140/T	Shorikha	YEN	0	ds				235	34		3302	0.49	4776	6.87	97		
K95-54	Miroyedikha	KAM	0	ds		0.8	−4.0	405	40		1963	0.51	4317	10.12	49		
K95-51	Miroyedikha	KAM	2	ds		0.8	−4.3	379	34		3035	0.57	4362	11.19	90		
K95-55	Miroyedikha	KAM	6	ds		1.1	−3.8	489	45		2913	0.52	3215	10.98	65		
K95-52	Miroyedikha	KAM	7	ds		0.2	−6.9	1248	49		4705	0.48	3415	25.36	96		
K95-56	Miroyedikha	KAM	11	ds		1.6	−3.5	480	319		6633	0.35	263	1.50	21		
K95-57	Miroyedikha	KAM	17	ds		1.3	−5.0	918	36		5375	0.49	4075	25.64	150		
K95-58	Miroyedikha	KAM	24	ds		1.2	−5.6	1125	30		4650	0.59	3880	37.93	157		
K95-59	Miroyedikha	KAM	32	ds		1.6	−5.4	1974	28		3628	0.55	5443	70.17	129		
K95-53	Miroyedikha	KAM	45	ds		2.3	−5.2	1453	23		2724	0.50	6319	63.15	118		
K95-60	Miroyedikha	KAM		ds		2.3	−5.0	1152	39		2958	0.52	3602	29.89	77		
K95-129-0	Miroyedikha	MIR	0	ds	1.6		−3.8	159	45		3341	0.61	2685	3.56	75		
K95-129-5	Miroyedikha	MIR	5	ds													
K95-129-10	Miroyedikha	MIR	10	ds	1.8		−3.8	280	46		3978	0.55	3226	6.16	87		
K95-129-15	Miroyedikha	MIR	15	ds													
K95-129-20	Miroyedikha	MIR	20	ds	1.5		−5.2										
K95-129-25	Miroyedikha	MIR	25	ds													
K95-129-30	Miroyedikha	MIR	30	ds		1.3	−5.1	994	59		12 646	0.41	2209	16.83	214		
K95-129-35	Miroyedikha	MIR	35	ds													
K95-129-40	Miroyedikha	MIR	40	ls	0.8		−8.4										
K95-129-45	Miroyedikha	MIR	45	ls													
K95-129-49	Miroyedikha	MIR	49	ds		1.2	−6.3	1731	54		8633	0.44	2454	32.18	161		
K95-129-57	Miroyedikha	MIR	57	ds		0.6	−5.4	8050	56		18 675	0.42	2416	144.72	336		
K95-129-129	Miroyedikha	MIR	129	ls		−1.1	−12.1	6412	83		16 242	0.04	2854	77.16	195		
K95-129-135	Miroyedikha	MIR	135	ds													
K95-129-140	Miroyedikha	MIR	140	ls				649	126	169	4444	0.05	1887	5.15	35	0.0134	
K95-129-149	Miroyedikha	MIR	149	ls	1.9		−5.2	513	99	130	14 611	0.29	1416	5.20	148	0.0340	
K95-129-155	Miroyedikha	MIR	155	ls				712	113	222	3984	0.11	1813	6.29	35	0.0181	
K95-129-170	Miroyedikha	MIR	170	ls		−0.9	−13.2	253	125		2322	0.02	2144	2.02	19		
K95-129-175	Miroyedikha	MIR	175	ls				131	120	210	2933	0.03	1907	1.09	24	0.0084	0.70753
K95-129-180	Miroyedikha	MIR	180	ls	2.5		−8.1			124						0.0018	0.70717
K95-129-191	Miroyedikha	MIR	191	ds		1.0	−5.3	2870	77		32 296	0.37	1923	37.35	420		
K95-129-195	Miroyedikha	MIR	195	ls				292	30		5806	0.43	4974	9.66	192		
K95-140-0	Miroyedikha	YEN	0	ds	2.0		−2.3	178	29		3058	0.53	4027	6.06	104		
K95-140-10	Miroyedikha	YEN	10	ds	1.9		−6.4	260	30		4340	0.53	4171	8.71	146		
K95-140-20	Miroyedikha	YEN	20	ds		1.3	−5.1	391	34		5091	0.44	4573	11.66	152		
K95-140-20	Miroyedikha	YEN	20	ds		1.5	−4.5										
K95-140-30	Miroyedikha	YEN	30	ds		0.6	−6.6	671	63		8771	0.40	1917	10.61	139		
K95-140-38	Miroyedikha	YEN	38	ls	1.2		−7.7	349	56	112	3360	0.09	2287	6.19	60	0.0083	0.70793
K95-140-38A	Miroyedikha	YEN	38	ls	1.1		−9.9	296	83		3396	0.01	3216	3.58	41		
K95-140-48	Miroyedikha	YEN	48	ds	1.7		−7.4										
K95-140-126	Miroyedikha	YEN	126	ls		0.7	−10.2										
K95-140-128	Miroyedikha	YEN	128	ls		1.6	−9.7	3795	95	150	11 023	0.06	1930	39.86	116	0.0330	
K95-140-135	Miroyedikha	YEN	135	ls	2.2		−9.6	992	341	307	3340	0.03	1288	2.91	10	0.0021	0.70688
K95-140-145	Miroyedikha	YEN	145	ds				224	42		2217	0.41	4179	5.39	53		
K95-140-155	Miroyedikha	YEN	155	ds	2.3		−7.0	217	43		2305	0.39	4020	5.05	54		
K95-140-168	Miroyedikha	YEN	168	ds	2.4		−5.4	459	51		8455	0.36	2868	8.92	164		
K95-140-177	Miroyedikha	YEN	177	ds	2.0		−7.2	393	72		6152	0.39	2336	5.50	86		
K95-139-1	Turukhansk	MIR	1	ds	3.6		−5.3	182	34		3349	0.57	4594	5.34	98		
K95-139-9	Turukhansk	MIR	9	ds	3.1		−5.8	99	19		2480	0.60	6718	5.31	134		
K95-139-17	Turukhansk	MIR	17	ds	2.9		−5.2	162	17		4106	0.55	7572	9.46	240		
K95-139-25	Turukhansk	MIR	25	ds	2.9		−5.8	85	16		2388	0.57	7291	5.47	154		

Table 1 (*Continued*)

Sample	Formation	Section	Height	Lithology	$\delta^{13}C$	$\delta^{13}C_{altered}$	$\delta^{18}O$	Mn (ppm)	Sr (ppm)	Sr (ID)	Fe (ppm)	Mg/Ca	Ca/Sr	Mn/Sr	Fe/Sr	Rb/Sr	$^{87}Sr/^{86}Sr$
K95-139-35	Turukhansk	MIR	35	ds	3.3		−5.6	235	24		2586	0.55	6796	9.73	107		
K95-139-45	Turukhansk	MIR	45	ds	2.7		−8.3	110	16		2280	0.59	7574	6.97	144		
K95-139-55	Turukhansk	MIR	55	ds	3.6		−4.6	42	18		1988	0.58	6750	2.31	109		
K95-139-65	Turukhansk	MIR	65	ds	2.7		−6.2	102	21	35	2097	0.58	4831	4.90	101	0.1139	
K95-139-88	Turukhansk	MIR	88	ds	3.4		−8.5	171	36		2169	0.54	4389	4.80	61		
K95-139-95	Turukhansk	MIR	95	ds	3.4		−5.4	99	22		2664	0.53	6082	4.50	122		
K95-139-105	Turukhansk	MIR	105	ds	2.9		−5.2	61	17		2189	0.55	7086	3.63	129		
K95-139-115	Turukhansk	MIR	115	ds	3.3		−5.0	64	21		2825	0.61	5868	3.11	136		
K95-139-125	Turukhansk	MIR	125	ds	3.3		−5.4	58	17		2207	0.59	6631	3.33	127		
K95-139-135	Turukhansk	MIR	135	ds				42	12		1388	0.56	7178	3.53	117		
K95-139-145	Turukhansk	MIR	145	ds	3.5		−4.6	56	22		2126	0.56	6533	2.52	95		
K95-142-1	Turukhansk	YEN	1	ds	3.0		−6.3	221	45		3714	0.49	3589	4.96	83		
K95-142-10	Turukhansk	YEN	10	ds	2.1		−8.6	192	44		2302	0.43	4006	4.34	52		
K95-142-20	Turukhansk	YEN	20	ds	3.0		−6.4	209	47		2058	0.40	3787	4.48	44		
K95-142-30	Turukhansk	YEN	30	ds	3.0		−6.8	167	41		2419	0.52	4127	4.05	59		
K95-142-40	Turukhansk	YEN	40	ds				202	29		3386	0.57	4879	6.93	116		
K95-142-50	Turukhansk	YEN	50	ds	2.8		−7.6	182	2265		2266	0.41	77	0.08	1		
K95-142-60	Turukhansk	YEN	60	ds	2.9		−6.5	281	45		2917	0.46	3826	6.29	65		
K95-142-65	Turukhansk	YEN	65	ds	2.6		−8.3	149	20		2721	0.54	6397	7.62	139		
K95-142-70	Turukhansk	YEN	70	ds		3.1	−6.1	482	34		4237	0.51	5038	14.13	124		
K95-142-75	Turukhansk	YEN	75	ds				959	30		6512	0.46	4038	31.82	216		
K95-142-104	Turukhansk	YEN	104	ds	3.5		−5.3	170	32		2854	0.39	5576	5.28	89		
K95-142-114	Turukhansk	YEN	114	ds	3.1		−6.5	139	26		2643	0.47	7113	5.44	103		
K95-142-124	Turukhansk	YEN	124	ds	3.4		−6.9	128	32	27	2458	0.60	5313	4.01	77	0.0068	
K95-142-134	Turukhansk	YEN	134	ds				123	22		2432	0.38	7920	5.56	110		
K95-142-144	Turukhansk	YEN	144	ds	2.8		−7.2	108	21		1937	0.43	7874	5.14	92		
K95-142-154	Turukhansk	YEN	154	ds		3.1	−10.1	124	24		1963	0.43	7431	5.09	81		
K95-142-164	Turukhansk	YEN	164	ds	2.6		−6.8	105	23		2063	0.48	6695	4.62	91		
K95-142-174	Turukhansk	YEN	174	ds	3.3		−4.4	73	26		1712	0.43	7116	2.85	66		
K95-142-187	Turukhansk	YEN	187	ds	3.7		−5.3	86	23		1713	0.40	6680	3.77	75		
K95-142-197	Turukhansk	YEN	197	ds				180	32		2744	0.52	5079	5.58	85		

Sample numbers beginning with K were collected on a joint US–Russian expedition in 1995 and were analyzed according to the protocol described in the text. Sample numbers beginning with T were collected previously and obtained as whole-rock powders. Stable isotopic and elemental data for these samples were reported in Knoll et al. (1995). Formation: formation from which sample was obtained. Section: location of section from which sample was obtained. CNTS – Central Nizhnyaya Tunguska section; KAM – Kammennaya-Bol'shaya Shorikha River section; ST – Sukhaya Tunguska River Section; MIR – Miroyedikha River section; YEN – Yenisei River Section. See Fig. 1 for section locations. Height: stratigraphic height (m) above local datum, generally the base of the local outcrop. Lithology: composition of the rock sample: ls – limestone; ds – dolostone. Stable isotopic data are reported in permil (‰) relative to PDB. Uncertainty is <0.1‰ for $\delta^{13}C$ and <0.3‰ for $\delta^{18}O$. Values of $\delta^{13}C$ are considered altered if $\delta^{18}O < -10$‰ or if $Mn/Sr > 10$ (see text for explanation). Elemental values are reported in $mg_{element}/g_{sample}$ (ppm). Standard errors for Ca, Mg, Mn, and Sr are less than 10%, based on multiple analyses of a laboratory standard. Standard error for Fe is less than 15%. Elemental ratios are reproducible with standard errors <5%. Detection limits for trace elements are as follows: Mn, $Sr < 15$ ppm; $Fe < 30$ ppm. Rb/Sr elemental ratios were determined by isotope dilution, and are reproducible to 0.0005, based on multiple analyses of samples. Sr isotopic ratios were determined by analysis of 500–1000 ng of purified Sr on a Finnigan 262 TIMS multiple analyses of NBS-987 Sr standard run during the course of this investigation averaged 0.710241 ± 0.000008.

mation along the Belaya River, 9–14 km downstream from the mouth of Svetlyi Creek (Samples UM29–UM44). The second set was collected in the northeastern part of the Uchur–Maya Plate (Fig. 2, Section 2), and represents the lower part of the Malgina Formation, near the mouth of the Aim River (Samples UM24–UM28), the Tsipanda Formation (Samples UM45–UM81), and the Lakhanda Group (Samples UM82–UM107), exposed along the Maya River at and downstream from the mouth of the Aim River.

4.2. Geochemical methods

Petrographic, elemental, and oxygen-isotopic tests of the degree of alteration of carbonate samples were carried out in the course of this investigation. These tests are described elsewhere in detail (Derry et al., 1992; Kaufman et al., 1993; Gorokhov et al., 1995; Kaufman and Knoll, 1995; Podkovyrov et al., 1998). In brief, thin and polished thick sections were prepared from all samples collected for this study. Samples obtained from the Turukhansk region on previous excursions (Knoll et al., 1995) were obtained as whole-rock powders. Because the aim of this study was to reconstruct primary seawater composition, subsamples of newly collected rocks from the Turukhansk region and of all samples from the Uchur–Maya region were selected to represent only the least-altered portions of rock. Thin sections were evaluated petrographically and thick sections were qualitatively assessed using cathodoluminescence. Samples showing bright luminescence (high Mn content) were regarded as geochemically suspect, and highly luminescent phases were avoided during sampling. Based on these assessments, individual carbonate phases were drilled from each thick section using 1 mm drill bits (Kaufman et al., 1991). Sampled phases include micrite, cement, and fabric-retentive carbonate textures, which generally represent primary to early diagenetic marine carbonate. In general, samples had homogeneous petrographic and luminescent characteristics on the scale at which they were drilled. Most of the rocks examined in this study lacked distinctive non-marine diagenetic fabrics such as zoned meteoric cements or late-stage spar.

Aliquots of drilled powders were weighed (typically <2 mg) and dissolved in ultraclean 0.5 M acetic acid. After dissolution, solutions were decanted, dried, and diluted in 2% HNO_3; residues were dried and weighed to determine percent dissolution. Major (Ca, Mg) and trace (Mn, Sr, Fe) element analyses of carbonates were performed on the Harvard University VG PQ2$^+$ ICP-MS. Gravimetrically determined standards were analyzed in order to develop response calibration curves and internal standards of 100 ppb ^{115}In (and 100 ppb ^{45}Sc for samples from the Turukhansk region) were added to each sample prior to analysis (Lea and Martin, 1996). Ca, Mg, Mn and Sr show reproducibility better than 10%. Fe measurements show reproducibility better than 15%. Comparison of Sr concentrations determined by ICP-MS with those analyzed by isotope dilution methods reveals a discrepancy between absolute values obtained, with Sr content determined by ICP-MS systematically lower than that obtained by isotope dilution, suggesting, perhaps, suppression of the Sr signal during ICP-MS analysis. Where evaluated, Sr concentrations are shown by both ID and ICP-MS techniques. Ratios among trace elements are reproducible, and yield standard errors of less than 5%.

Microsampled limestones were reacted with $>102\%$ H_3PO_4 ($\rho > 1.89$ g/ml) at 90°C in the auto-sample magazine of the VG PRISM gas source isotope ratio mass spectrometer at Harvard University for the determination of C and O isotopic compositions. Because a longer reaction time is necessary for the quantitative digestion of dolomites, these samples were dissolved using off-line techniques under identical conditions and were isolated by cryogenic distillation. Fractionation factors used for the calculation of ^{18}O abundances of calcite and dolomite based on analyses of CO_2 prepared at 90°C were 1.00798 and 1.00895, respectively (Sharma and Clayton, 1965). Standard error for these isotopic techniques as determined by multiple determinations ($n > 50$) of calcite and dolomite standards is $<0.1‰$ for C and $<0.3‰$ for O.

For Sr isotopic analyses, < 5 mg samples of powder were dissolved in ultraclean 0.5 M acetic acid. A small aliquot of the resulting solution was extracted and spiked with isotopic tracers for Rb and Sr. Rb/Sr ratios were determined by isotope dilution methods on the Finnigan Thermoquad at Harvard University. Sr was isolated from the remaining solution using standard ion exchange resins. 500–1000 ng of purified Sr was then loaded onto a Ta filament with 1 μm H_3PO_4 for TIMS analysis on the Harvard University Finnigan 262 multicollector mass spectrometer. Multiple analyses of NBS-987 Sr standard run during the course of this investigation averaged 0.710241 ± 0.000008 (uncertainty given as 2σ of the mean).

For several of the samples from the Uchur–Maya region, a second aliquot of carbonate powder was treated with ammonium acetate ($CH_3COO^-NH_4^+$) to remove adsorbed and loosely bound Sr, then processed as above and analyzed on the VG Sector 54 TIMS at the University of Maryland. Multiple analyses of NBS-987 Sr standard averaged 0.710244 ± 0.000017 (uncertainty given as 2σ of the mean). This method has been shown to maximize likelihood of recovering initial $^{87}Sr/^{86}Sr$ values in Proterozoic (Gorokhov et al., 1995, 1996a,b; Gorokhov, 1996; Kuznetsov et al., 1997a,b, 1998a,b; Semikhatov et al., 1998a,b) and Paleozoic (e.g., Montañez et al., 1998) carbonates. $^{87}Sr/^{86}Sr$ values for samples prepared in this manner are reported in a separate column in Table 1. It should be emphasized that, given generally low Rb content in all studied samples and significant age uncertainty, measured $^{87}Sr/^{86}Sr$ ratios are not corrected for age. If applied, such corrections would be in the fifth decimal place, at the limit of our ability to interpret the data. Data of Gorokhov et al. (1995) have been so corrected.

5. Results

5.1. Diagenesis and preservation of carbonate geochemical signatures

Variation in trace element concentration and oxygen isotopic composition of carbonate rocks reveal diagnostic alteration trends that result from interaction with diagenetic fluids (Brand and Veizer, 1980; Banner et al., 1988; Banner and Hanson, 1990; Jacobsen and Kaufman, 1999). The difference in composition between a carbonate rock (and the water from which it precipitated) and a diagenetic fluid is the primary factor in determining the rate and extent of elemental and isotopic exchange in the carbonate rock. Several theoretical, experimental, and analytical studies of carbonate diagenesis have been undertaken over the past two decades (e.g., Brand and Veizer, 1980; Veizer, 1983; Banner and Hanson, 1990; Banner, 1995; Gorokhov, 1996; Jacobsen and Kaufman, 1999), and some generalizations about carbonate alteration have emerged. However, each succession of carbonates will have a unique history of diagenetic alteration that can be elucidated only by petrographic and geochemical study of each succession within the framework of diagenesis.

Despite the obvious complexity of the carbonate system and questions as to the interpretation of diagenetic signals, the goal of this study is to extend the database for a currently inadequately understood interval of earth history, and to evaluate broad, long-term trends in seawater composition. We have therefore chosen a manifold approach to ensuring analysis of diagenetically *least altered*, though not necessarily *unaltered* carbonate components: (1) primary screening using petrology – obviously recrystallized phases are avoided during sampling; (2) cathodoluminescence analysis of polished thick sections. Areas that are highly luminescent are not sampled; (3) microdrilling of least-altered phases, to avoid contamination of samples with obviously altered carbonate; (4) C and O isotopic analysis, using $\delta^{18}O$ values as a coarse indicator of likely alteration in $\delta^{13}C$; (5) elemental analysis to reveal highly altered samples ($Mn/Sr > 10$) with disturbed C isotopic systems; (6) careful evaluation of elemental data to reveal diagenetic trends within or among units in a region, to increase the likelihood of recovering primary $^{87}Sr/^{86}Sr$ values; and (7) evaluation of isotopic data within their stratigraphic context, to determine whether the observed patterns represent a plausible record of seawater composition.

With the goal of reconstructing broad trends in seawater composition, we sampled only dully luminescent, early carbonate phases in each sample, then applied geochemical screening criteria to each sample to evaluate the potential reliability of $\delta^{13}C$ and $^{87}Sr/^{86}Sr$ data. Because $\delta^{13}C$ values in carbonates typically change more slowly during diagenesis than do $\delta^{18}O$ or Mn/Sr values, we adhere to empirically determined guidelines (Knoll et al., 1995) and have designated all samples with $\delta^{18}O$ values $< -10‰$ or with Mn/Sr ratios >10 as 'altered' and thus unlikely to reliably record seawater C isotopic values.

Significant evidence, however, suggests that the Sr isotopic system is more sensitive to secondary alteration of carbonate rocks than are C isotopic values (Derry et al., 1992; Gorokhov et al., 1995; Montañez et al., 1998; Ovchinnikova et al., 1998). Therefore, a more stringent set of criteria must be applied when discussing the potential preservation of seawater $^{87}Sr/^{86}Sr$ values. Because diagenetic alteration depends upon the composition of the original carbonate as well as the composition of the diagenetic fluid, it is likely impossible to devise a single set of criteria that will be applicable to all Proterozoic carbonates, and each succession must be independently evaluated within its depositional and diagenetic context. In this study, we considered limestones to be unaltered when $Mn/Sr < 1.5$ and $Rb/Sr < 0.01$. Because most dolostones have low Sr abundances, due to crystallographic exclusion of Sr, we consider dolostones to be unaltered when $Mn/Sr < 3.0$ and $Rb/Sr < 0.01$. In certain cases (Table 1), ideal samples were simply not preserved within studied suites, and sub-optimal samples, representing the least altered within a formation, were analyzed in order to obtain a maximum constraint on $^{87}Sr/^{86}Sr$. Although analysis of the data in this way does not ensure the recovery of primary Sr isotopic values, it does increase the likelihood of reconstructing seawater composition on a broad time scale.

5.1.1. Turukhansk region

Fig. 4 shows formation-specific trace element and isotopic data for carbonates of the Turukhansk region, analyzed in this study. The following broad diagenetic trends are evident. Carbonates of the Sukhaya Tunguska and Burovaya Formations exhibit the least degree of diagenetic alteration, with high Sr/Ca ratios, low Mn content, uniform $\delta^{18}O$ values, and relatively low Fe content. Carbonates of the Linok Formation show mainly little-altered $\delta^{18}O$ values, between $-5‰$ and $-7‰$ and generally low Mn/Sr values. Several samples have high Mn content. These samples represent an organic-rich, possibly anoxic facies within the Linok Formation. Dolostones of the Turukhansk Formation have generally uniform $\delta^{18}O$ values, near $-6‰$, with a few samples showing ^{18}O depletion. Carbonates of the Miroyedikha Formation exhibit a wide range of alteration characteristics. The most highly altered samples have suffered severe enrichment in Fe and Mn, and have low $\delta^{18}O$ values. The Derevnya and Shorikha Formations display variable, and mostly intermediate, degrees of alteration.

5.1.2. Uchur–Maya region

Most samples from the Uchur–Maya retain $\delta^{18}O$ signatures near average marine values for Proterozoic carbonates (from $-4‰$ to $-7‰$), but preserve a wide range of values in other diagenetic indicators (Fig. 5). Overall, seawater $\delta^{13}C$ values are likely preserved in all units of the Uchur–Maya region, but $^{87}Sr/^{86}Sr$ values likely only provide maximum constraints on seawater composition. Best-preserved samples, which come from the Neryuen Formation, have high Sr/Ca ratios, low Mn/Sr ratios, and low Fe content. Thus, we consider the limestones of the Neryuen Formation to be most likely to record primary seawater $^{87}Sr/^{86}Sr$ ratios. Other units must be regarded as altered to varying degrees by post-depositional processes, yielding only a maximum value for coeval seawater Sr isotopic composition. This post-depositional alteration is most noticeable in an overall Mn and Fe enrichment in upper Malgina Formation carbonates, and as iron enrichment in Tsipanda and Ignikan carbonates. However, carbonates of the lower

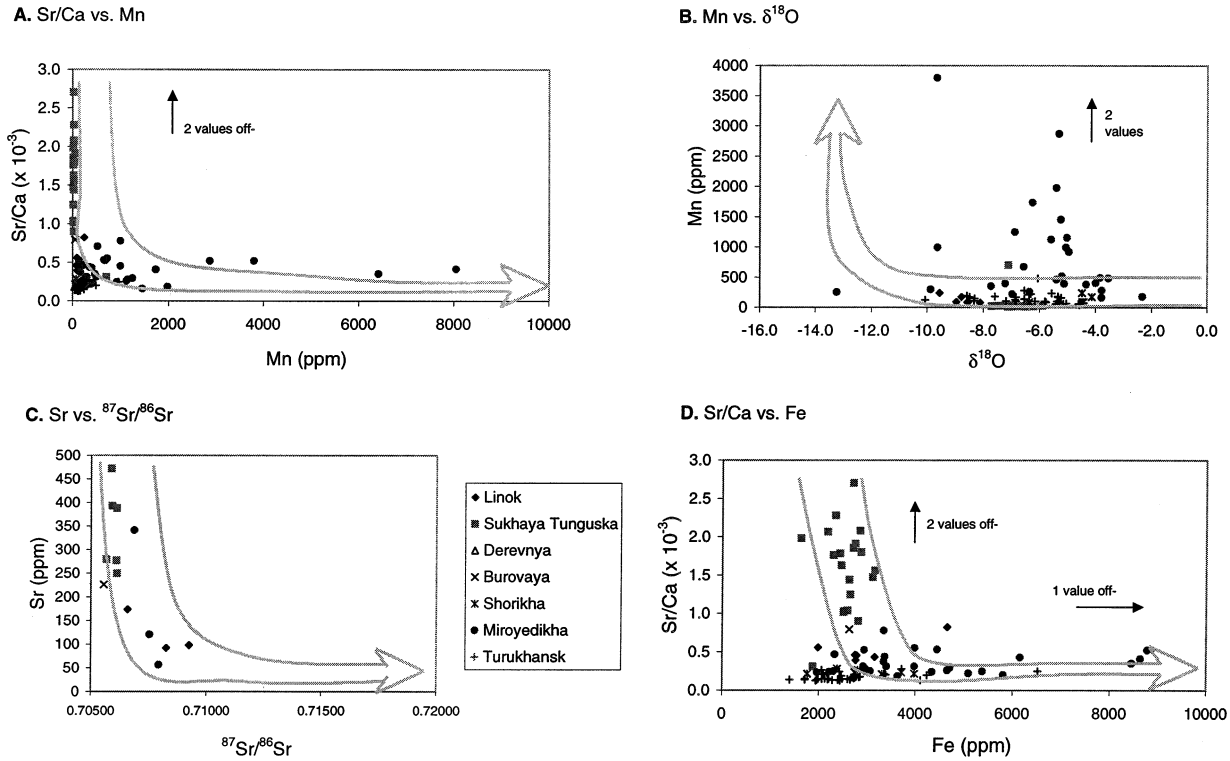

Fig. 4. Cross-plots of elemental data from the Turukhansk region. Data are separated by formation. (A) Sr/Ca elemental ratio vs. Mn concentration (ppm). Off-scale values are samples from the Turukhansk and Miroyedikha Formations. (B) Mn concentration (ppm) vs. $\delta^{18}O_{PDB}$. Off-scale values are samples from the Miroyedikha Formation. (C) Sr concentration (ppm) vs. $^{87}Sr/^{86}Sr$. (D) Sr/Ca elemental ratio vs. Fe concentration (ppm). Gray arrows indicate generalized alteration trends during meteoric diagenesis (Banner and Hanson, 1990).

mation contain a sub-population of closely spaced samples near the base of the unit with tightly clustered $^{87}Sr/^{86}Sr$ values. Such clusters of minimum $^{87}Sr/^{86}Sr$ may be used to constrain a maximum value for coeval seawater.

5.2. Carbon isotope chemostratigraphy

5.2.1. Turukhansk region

New C isotopic data from the Turukhansk region were obtained from the lower Linok Formation (Kammennaya River section), lower Sukhaya Tunguska Formation (Kammennaya and Sukhaya Tunguska River sections), Burovaya Formation (Kammennaya River section), Miroyedikha Formation (Bol'shaya Shorikha, Miroyedikha, and Yenisei River sections), and the Turukhansk Formation (Miroyedikha and Yenisei River sections). In the lower formations, sampling focused on texturally well-preserved limestones and improved stratigraphic resolution (5–10-m intervals). This sampling strategy permits construction of a carbon-isotopic curve for this part of the section that was largely represented by altered samples, based on $\delta^{18}O$ and trace element data (Knoll et al., 1995). The upper units (Miroyedikha and Turukhansk Formations) were closely sampled (5–10-m intervals), with the aim of identifying regions of rapid chemostratigraphic change.

These data are reported in Tables 1 and 3, and are included in Figs. 6–9, along with previously published data from this region (Knoll et al., 1995). In general, the Riphean carbonates of the Turukhansk region exhibit several major secular trends in $\delta^{13}C$ (Fig. 9). The Linok Formation

(Fig. 6, Table 3) commences with moderately positive $\delta^{13}C$ values, followed by a rapid fall to negative values, near −2‰. Upsection, $\delta^{13}C$ values increase from about −2‰ to ~0‰ with a previously unrecognized higher-order variation superimposed on an overall rise. Scattered samples of the upper part of the Linok Formation indicate slightly negative $\delta^{13}C$ values. The lower Sukhaya Tunguska Formation displays several shifts between 0‰ and +3‰, expressed as an ascending trend with superimposed variation (Fig. 6, Table 3). The upper part of the formation records a broad negative excursion, to values as low as −2.7‰, followed by a rise to values near 0‰ near the top of the unit. Carbonates above the sub-Derevnya erosional surface have predominantly positive $\delta^{13}C$ values. Average values in the Derevnya, Burovaya and lower Shorikha carbonates (Fig. 7) are moderately positive, and maximum values exceed +4.5‰ (Table 3). Little high-frequency change is evident at current sampling resolution, although one prominent negative excursion (to −2.4‰) occurs in the lower part of the Derevnya Formation. A strong negative excursion is observed in the upper Shorikha Formation, to values as light as −5‰. Within this excursion, $\Delta\delta C$ values ($\delta^{13}C_{carb} - \delta^{13}C_{org}$) are reduced (25–27‰) relative to $\Delta\delta C$ values throughout the rest of the succession (~30‰; Knoll et al., 1995), suggesting that diagenetic exchange of organic matter with carbonate C is in part responsible for the excursion, and that primary C isotopic values in the upper Shorikha Formation are likely only moderately negative. From the uppermost Shorikha Formation into the lower Miroyedikha Formation, $\delta^{13}C$ values rise from near 0‰ to +2.3‰, drop briefly to values near 0‰ in the upper Miroyedikha Formation, then rise steadily through the Turukhansk Formation, culminating in a value of +4.2‰ near the top of the unit (Fig. 8). Despite intense sampling, little high-order variation is detectable in these uppermost formations.

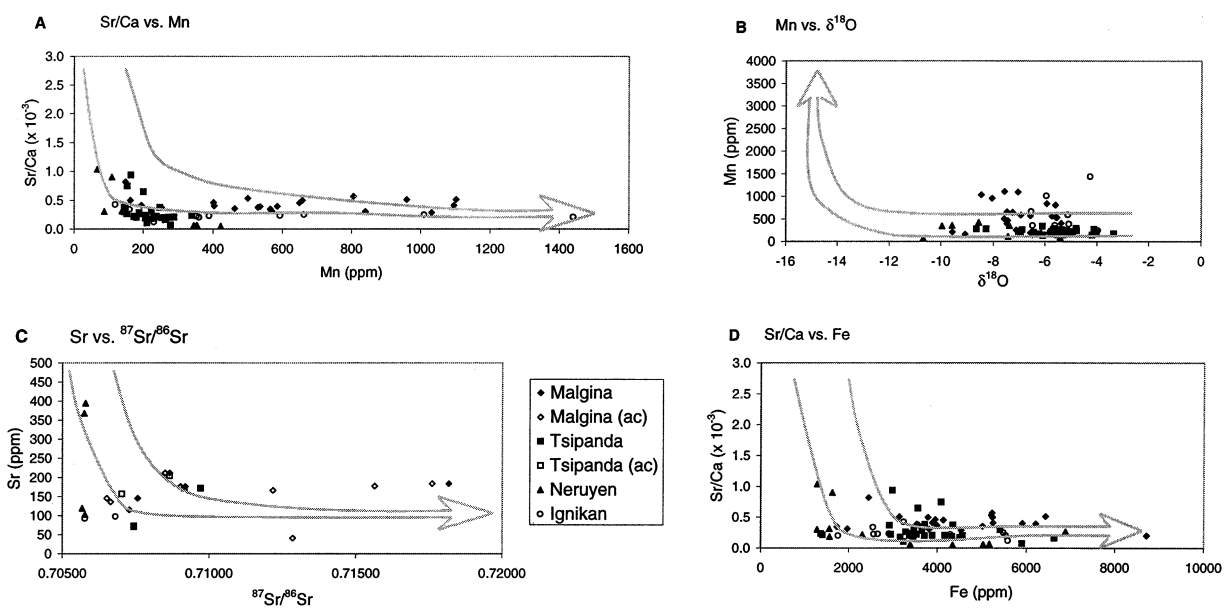

Fig. 5. Cross-plots of elemental data from the Uchur–Maya region. Data are separated by formation. The designation (ac) in the legend indicates that samples were treated with ammonium acetate prior to dissolution. (A) Sr/Ca elemental ratio vs. Mn concentration (ppm). (B) Mn concentration (ppm) vs. $\delta^{18}O_{PDB}$. (C) Sr concentration (ppm) vs. $^{87}Sr/^{86}Sr$. (D) Sr/Ca elemental ratio vs. Fe concentration (ppm). Gray arrows indicate generalized alteration trends during meteoric diagenesis (Banner and Hanson, 1990).

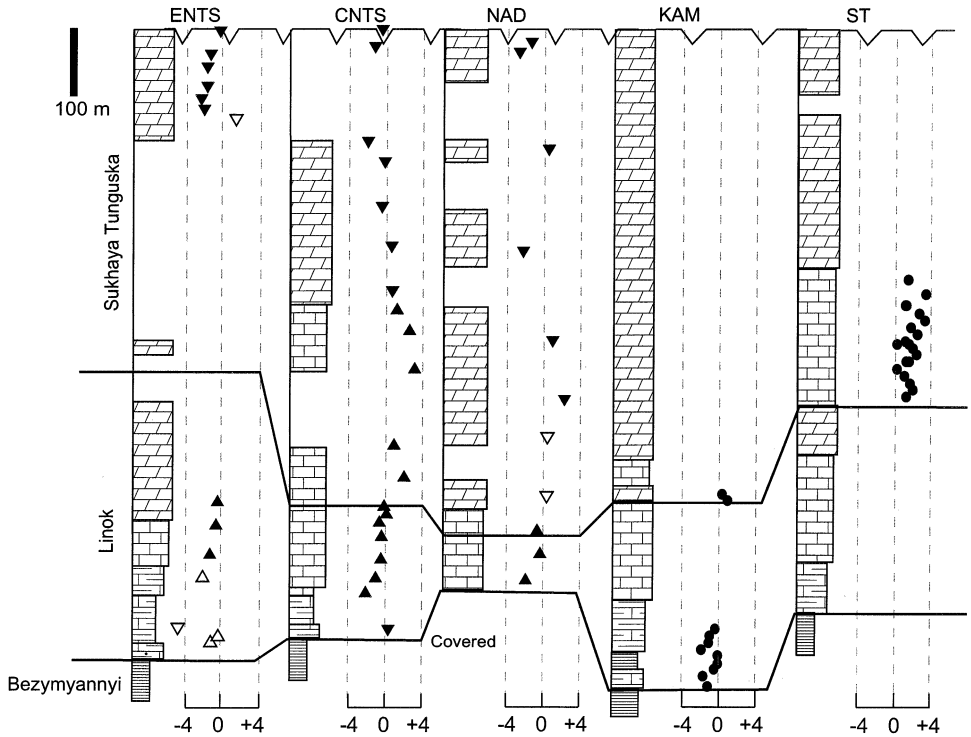

Fig. 6. Carbon isotope chemostratigraphy for the Linok and Sukhaya Tunguska Formations of the Turukhansk Uplift. Data plotted include analyses of this study (circles) as well as previously published data (Knoll et al., 1995; triangles). Legend is given in Fig. 7. Stratigraphic sections are as given for Table 1, with two additions: NAD refers to the Nadporozhnyaya River section, and ENTS refers to the Eastern Nizhnyaya Tunguska River section.

5.2.2. Uchur–Maya region

Carbon isotopic data from the Uchur–Maya region shows a pattern of nearly invariant $\delta^{13}C$ values in the sub-Lakhanda part of the succession (Fig. 10, Tables 2 and 4). The little-altered dolostones in the Svetlyi Formation have $\delta^{13}C$ values between $-0.6‰$ and $+1.1‰$. Likewise, most $\delta^{13}C$ values of the sampled portion of the Malgina Formation along the Belaya River (northern Yudoma–Maya Belt) cluster near 0‰ (Fig. 10), with two samples in the upper part of the unit documenting a positive shift up to $+1.9‰$ (Tables 2 and 4). Samples obtained from the Malgina Formation along the Aim River (Uchur–Maya Plate) record an increase in $\delta^{13}C$ values from $-1.9‰$ near the base of the formation (Vinogradov et al., 1998) to moderately positive values ($+1.0‰$). Above this, the stratigraphic pattern suggests a second negative-to-positive excursion, delineated by only a few samples (this study; Vinogradov et al., 1998). The overlying Tsipanda Formation, closely sampled in the Maya River section, is characterized by a conspicuous lack of stratigraphic variation; $\delta^{13}C$ values are slightly positive, between $+0.5$ and $+1.7‰$ (Fig. 10, Tables 2 and 4).

In contrast, carbonates above the sub-Lakhanda unconformity exhibit a markedly different pattern of secular variation (Fig. 10, Table 4). Our samples of the lower Lakhanda Neryuen Formation, collected along the Maya River within the Uchur–Maya Plate, come from the middle carbonate member of the formation. $\delta^{13}C$ values for this middle member lie between $-2.8‰$ and $+3.1‰$, and little altered samples have $\delta^{13}C$ values between $+0.7‰$ and $+3.1‰$. Published data from the same section (Vinogradov et al., 1998) indicate a maximum $\delta^{13}C$ value of $+5‰$, mea-

Table 2
Geochemical data for new analyses of samples from the Uchur–Maya region

Sample	Formation	Section	Height	Lithology	$\delta^{13}C$	$\delta^{13}C_{altered}$	$\delta^{18}O$	Mn (ppm)	Sr (ppm)	Sr (ID)	Fe (ppm)	Mg/Ca	Ca/Sr	Mn/Sr	Fe/Sr	Rb/Sr	$^{87}Sr/^{86}Sr$	$^{87}Sr/^{86}Sr_{(ac)}$
UM-1	Treghorkha	Belaya	160	ds		−2.8	−10.6	627	87		25 868	0.23	2288	7.2	297			
UM-2	Treghorkha	Belaya	164	ds		−3.1	−10.7	414	49		14 603	0.25	2222	8.5	298			
UM-5	Treghorkha	Belaya	780	ds	−0.3		−5.8	1030	123		6768	0.34	2593	8.4	55			0.73774
UM-6	Treghorkha	Belaya	850	ds		−1.0	−5.6	2085	133		20 043	0.46	1368	15.7	151			
UM-7	Treghorkha	Belaya	1020	ls		−0.6	−5.7	1677	111		45 248	0.17	3946	15.1	408			
UM-7b	Treghorkha	Belaya	1020	ds		−1.0	−5.5	1845	126		38 434	0.30	2506	14.7	306			
UM-8	Svetlyi	Belaya	15	ds		0.4	−6.5	1829	146		18 494	0.48	1411	12.6	127			
UM-9	Svetlyi	Belaya	26	ds		−0.3	−5.5	769	45		4451	0.56	4406	17.0	98			
UM-10	Svetlyi	Belaya	35	ds		−1.1	−5.8	844	68		5130	0.48	3392	12.4	76			
UM-11	Svetlyi	Belaya	45	ds		0.5	−5.6	618	36		2743	0.57	5845	17.4	77			
UM-12	Svetlyi	Belaya	54	ds	0.5		−6.0	487	56		3851	0.44	4472	8.7	69			
UM-13	Svetlyi	Belaya	65	ds	0.7		−5.7	430	46		2856	0.56	5015	9.4	63			
UM-14	Svetlyi	Belaya	75	ds	−0.6		−5.9	224	75		3936	0.36	2896	3.0	53			
UM-15	Svetlyi	Belaya	90	ds	0.4		−6.9	325	51		2831	0.54	4265	6.4	55			
UM-16	Svetlyi	Belaya	120	ds	0.4		−6.3	361	55		3152	0.55	3741	6.6	58			
UM-17	Svetlyi	Belaya	145	ds	−0.4		−7.4	564	60		4872	0.51	4605	9.4	81			
UM-18	Svetlyi	Belaya	180	ds	1.1		−7.5	275	49		2894	0.56	4046	5.6	59			
UM-19	Svetlyi	Belaya	210	ds	−0.1		−5.9	302	68		4891	0.52	3319	4.4	72			
UM-20	Svetlyi	Belaya	240	ds	0.6		−6.3	186	58		3046	0.55	4087	3.2	53			
UM-21	Svetlyi	Belaya	270	ds	0.8		−6.6	131	72		1465	0.58	1736	1.8	20			
UM-21	Svetlyi	Belaya	270	ds	0.5		−6.5	151	59		1614	0.57	2984	2.6	28			
UM-22	Svetlyi	Belaya	300	ds	0.9		−6.9	211	118		2455	0.56	1704	1.8	21			0.72528
UM-23	Svetlyi	Belaya	325	ds	0.4		−8.2	654	165		6664	0.53	1337	4.0	40			
UM-24	Malgina	Maya	7	ls	−0.1		−5.6	536	146	170	3529	0.01	2575	3.7	24	0.0092	0.70757	0.70651
UM-25	Malgina	Maya	8.5	ls	0.0		−5.5	530	135		3572	0.01	2662	3.9	26			0.70664
UM-26	Malgina	Maya	16	ls	0.7		−5.9	839	115		3813	0.01	3289	7.3	33			0.70728
UM-27	Malgina	Maya	21	ls	0.7		−6.9	585	124		6214	0.01	2541	4.7	50			
UM-27b	Malgina	Maya	21	ds	1.0		−6.5	148	184		2442	0.51	1220	0.8	13			
UM-28	Malgina	Maya	25	ls	0.1		−6.6	570	104		1968	0.01	3217	5.5	19			
UM-28b	Malgina	Maya	25	ls	0.4		−5.7	565	121		1726	0.01	2900	4.7	14			
UM-29	Malgina	Belaya	55	ls	0.1		−7.5	657	176	224	3787	0.01	2013	3.7	22	0.0005	0.70917	0.70903
UM-30	Malgina	Belaya	80	ls	−0.3		−9.1	162			5230	0.01	2013	4.7	32			
UM-31	Malgina	Belaya	105	ls	0.1		−7.3	648	161		4131	0.01	2203	4.0	26			
UM-32	Malgina	Belaya	130	ls				894	179		3657	0.01	1960	5.0	20			
UM-33	Malgina	Belaya	155	ls	−0.3		−9.6	211	41		8719	0.02	4960	5.2	213			0.71284
UM-34	Malgina	Belaya	180	ls	−0.1		−8.1	959	177		6433	0.01	1953	5.4	36			0.71564
UM-35	Malgina	Belaya	205	ls	−0.1		−7.1	1096	183	249	5242	0.01	2433	6.0	29	0.0090	0.71818	0.71762
UM-36	Malgina	Belaya	230	ls	0.0		−6.6	194	160		3886	0.01	2420	1.2	24			
UM-37	Malgina	Belaya	255	ls	−0.3		−7.1	251	149		3984	0.01	2696	1.7	27			
UM-38	Malgina	Belaya	280	ls	0.3		−5.4	403	162		5910	0.02	2481	2.5	37			
UM-39	Malgina	Belaya	305	ls	0.2		−7.5	401	162		3949	0.01	2174	2.5	24			
UM-40	Malgina	Belaya	330	ls	1.6		−7.5	463	162		5004	0.01	2819	2.9	31			
UM-41	Malgina	Belaya	355	ls	1.9		−5.6	806	211	224	5218	0.01	1760	3.8	25	0.0009	0.70866	0.70850
UM-42	Malgina	Belaya	380	ls	0.6		−7.6	500	153		5200	0.01	1881	3.3	34			
UM-43	Malgina	Belaya	400	ls	0.3		−7.6	1102	166		3138	0.01	1959	6.6	19			0.71217

Table 2 (*Continued*)

Sample	Formation	Section	Height	Lithology	$\delta^{13}C$	$\delta^{13}C_{altered}$	$\delta^{18}O$	Mn (ppm)	Sr (ppm)	Sr (ID)	Fe (ppm)	Mg/Ca	Ca/Sr	Mn/Sr	Fe/Sr	Rb/Sr	$^{87}Sr/^{86}Sr$	$^{87}Sr/^{86}Sr_{(ac)}$
UM-44	Malgina	Belaya	420	ls	−0.5		−8.5	1032	146		4529	0.01	3485	7.1	31			
UM-45	Tsipanda	Maya	10	ds	1.3		−3.4	173	40		1400	0.58	4681	4.4	35			
UM-46	Tsipanda	Maya	17	ds	1.7		−4.8	237	44		2943	0.57	4540	5.4	67			
UM-47	Tsipanda	Maya	23	ds	0.8		−5.6	287	57		4166	0.43	4855	5.1	74			
UM-48	Tsipanda	Maya	30	ls	0.6		−6.1	339	70	390	1359	0.04	4268	4.8	19	0.0017	0.70744	
UM-49	Tsipanda	Maya	36	ds	1.1		−5.0	223	73	118	3470	0.47	3283	3.1	48	0.0074	0.70744	
UM-50	Tsipanda	Maya	40	ds	1.3		−5.2	180	40	52	4561	0.60	4991	4.5	113	0.0139		
UM-50	Tsipanda	Maya	40	ds	1.1		−7.0	221	38	46	3159	0.54	5665	5.8	83	0.0094		
UM-51	Tsipanda	Maya	49	ds	1.1		−5.6	253	44	52	3427	0.52	5166	5.7	78	0.0060		
UM-54	Tsipanda	Maya	68	ds	0.9		−5.4	263	38		6632	0.53	6292	7.0	176			
UM-55	Tsipanda	Maya	75	ds	1.7		−8.3	276	49		3708	0.52	5009	5.7	76			
UM-56	Tsipanda	Maya	82	ds	1.5		−4.1	271	47		3372	0.51	4868	5.8	72			
UM-57	Tsipanda	Maya	88	ds	0.9		−4.8	287	43		3879	0.56	4871	6.8	91			
UM-58	Tsipanda	Maya	95	ds	0.5		−5.2	172	45		3532	0.55	4564	3.8	78			
UM-59	Tsipanda	Maya	101	ds	0.6		−6.4	207	50		3390	0.55	4220	4.1	67			
UM-60	Tsipanda	Maya	108	ds	0.8		−5.7	264	35		4506	0.56	5909	7.6	130			
UM-61	Tsipanda	Maya	114	ds	0.9		−5.0	205	48		3456	0.50	5333	4.3	72			
UM-63	Tsipanda	Maya	127	ds	1.3		−4.0	200	156		3559	0.48	1553	1.3	23			0.70702
UM-64	Tsipanda	Maya	134	ds	1.2		−4.2	144	72		5404	0.52	3381	2.0	75			
UM-65	Tsipanda	Maya	140	ds	1.0		−5.0	188	66		3651	0.54	3550	2.8	55			
UM-67	Tsipanda	Maya	153	ds	1.0		−6.1	144	77		2911	0.52	2698	1.9	38			
UM-70	Tsipanda	Maya	170	ds		0.5	−8.7	278	14		5895	0.59	14 031	19.5	414			
UM-70	Tsipanda	Maya	170	ds	1.0		−6.9	210	23		3232	0.57	9652	9.2	141			
UM-71	Tsipanda	Maya	190	ds	0.9		−6.3	163	204	99	2974	0.51	1070	0.8	15	0.0098		0.70866
UM-73	Tsipanda	Maya	230	ds	1.1		−5.8	153	171	186	4078	0.53	1343	0.9	24	0.0077	0.70970	0.70915
UM-75	Tsipanda	Maya	118	ds	0.6		−5.5	152	56		3283	0.50	3848	2.7	58			
UM-76	Tsipanda	Maya	143	ds	0.7		−5.2	248	78		4346	0.52	2672	3.2	56			
UM-78	Tsipanda	Maya	160	ds	0.5		−5.3	148	91		3717	0.50	2620	1.6	41			
UM-81	Tsipanda	Maya	225	ds	0.7		−6.9	262	41		4324	0.57	5433	6.4	106			
UM-82	Neruen	Maya	0.5	ls	1.2		−5.8	225	83		1559	0.01	5369	2.7	19			
UM-85	Neruen	Maya	6.5	ls	0.7		−6.4	206	89		2307	0.02	4628	2.3	26			
UM-86	Neruen	Maya	21	ds	2.3		−6.2	194	61		6884	0.45	3796	3.2	113			
UM-87	Neruen	Maya	27	ls		2.6	−10.7	65	394	449	1277	0.01	965	0.2	3	0.0001	0.70577	
UM-89	Neruen	Maya	39	ls	3.1		−7.4	108	368	336	1622	0.02	1111	0.3	4	0.0001	0.70573	
UM-90	Neruen	Maya	44	ls	1.0		−5.4	86	118	147	1279	0.01	3319	0.7	11	0.0003	0.70566	
UM-91	Neruen	Maya	50	ls	0.7		−6.1	138	102		1557	0.08	3196	1.3	15		0.70576	
UM-92	Neruen	Maya	54	ds		−0.4	−9.6	352	15		5157	0.46	15 306	23.7	347			
UM-93	Neruen	Maya	60	ds		1.1	−7.4	354	12		5019	0.55	18 138	30.2	428			
UM-94	Neruen	Maya	67	ds		−2.8	−10.0	344	12		3386	0.56	16 948	28.4	280			
UM-95	Neruen	Maya	72	ds		1.7	−8.6	423	11		4343	0.56	20 859	38.3	393			
UM-96	Ignikan	Maya	9	ls	0.8		−5.1	593	92	156	2906	0.02	4306	6.4	32	0.0003	0.70576	
UM-97	Ignikan	Maya	25	ls	0.8		−5.6	359	82		1756	0.01	4958	4.4	21			
UM-98	Ignikan	Maya	35	ls	1.1		−5.1	388	97	144	2647	0.02	4380	4.0	27	0.0019	0.70681	
UM-99	Ignikan	Maya	45	ls		0.3	−4.3	1439	66		39 732	0.21	4824	21.8	602			
UM-100	Ignikan	Maya	50	ls	−0.1		−6.5	662	71		12 651	0.09	3992	9.3	177			
UM-101	Ignikan	Maya	55	ls	1.1		−6.5	352	82	96	2559	0.02	4471	4.3	31	0.0049		
UM-102	Ignikan	Maya	60	ds	2.9		−7.0	230	27		5579	0.42	8317	8.4	203			
UM-103	Ignikan	Maya	75	ls		−0.7	−6.0	1010	93		5482	0.01	4044	10.8	59			
UM-104	Ignikan	Maya	85	ds	3.6		−6.3	160	91		2544	0.33	2973	1.8	28			
UM-105	Ignikan	Maya	115	ds	1.2		−5.4	118	91		3237	0.47	2355	1.3	36			
UM-106	Ignikan	Maya	145	ds	1.6		−5.3	217	45		4294	0.55	4566	4.8	95			
UM-106b	Ignikan	Maya	160	ds	1.1		−4.0	241	39		5529	0.55	4867	6.2	143			

Samples were collected from two sections, the Belaya River section, and the Maya River section. Data from the Lower Riphean Tregorkha Formation (Uchur Group) were analyzed and are reported for completeness, though not discussed in the text. Abbreviations, uncertainties, and detection limits are the same as those given in Table 1. $^{87}Sr/^{86}Sr_{(ac)}$ refers to Sr isotopic analyses performed after pre-treatment of microsamples with ammonium acetate. These analyses were conducted on the VG Sector 54 TIMS at the University of Maryland. Multiple analyses of NBS-987 Sr standard averaged 0.710244 ± 0.000017.

sured in a single sample, from the lower part of the carbonate member. The precise stratigraphic position of the sample is, however, presently unresolved, and thus these data cannot be correlated in detail with results of the present study. $\delta^{13}C$ values as low as $-2.7‰$ (Vinogradov et al., 1998), are present in the lowermost part of the member, which is not represented in our data set.

The least altered samples of the upper Lakhanda Ignikan Formation yield predominantly moderately positive $\delta^{13}C$ values, between $-0.1‰$ and $+3.6‰$, with maximum $\delta^{13}C$ values occurring in the middle of the formation (Fig. 10). It should be noted that scattered samples collected in the carbonate-dominated section of the Lakhanda Group exposed along the Belaya River (Northern Yudoma–Maya Belt; Podkovyrov and

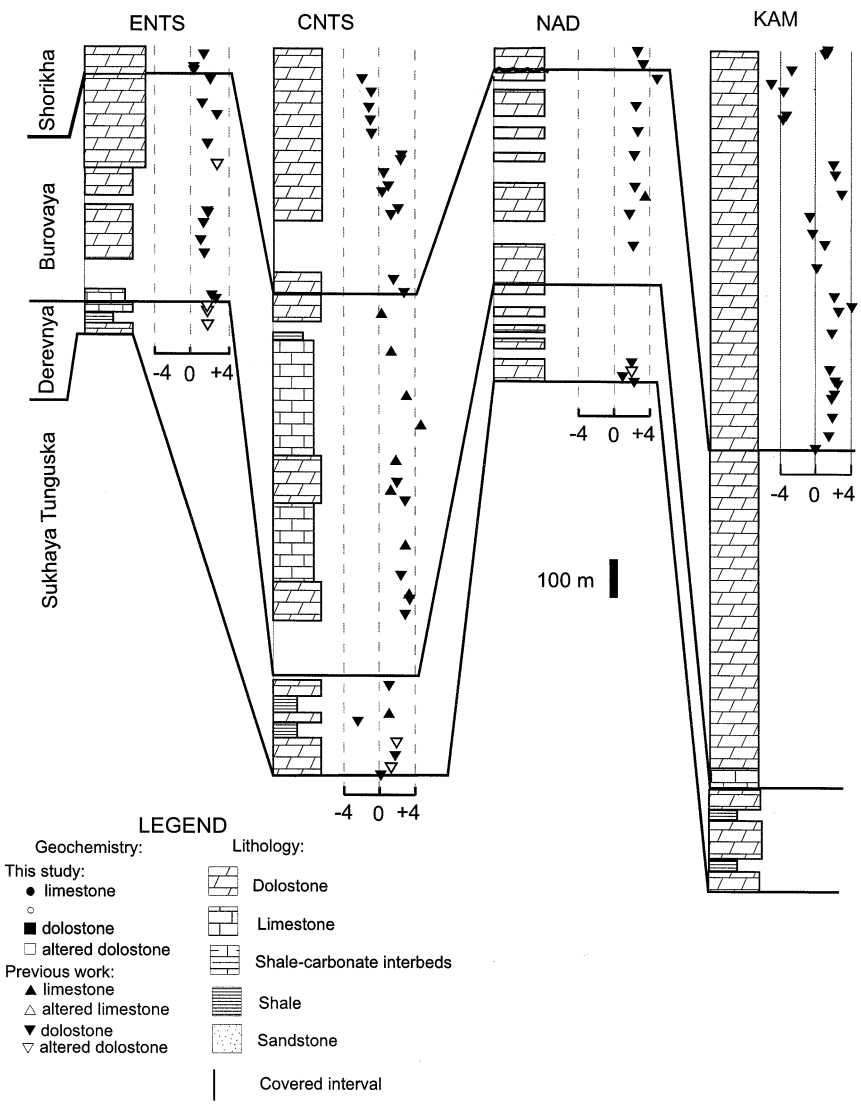

Fig. 7. Carbon isotope chemostratigraphy for the Derevnya, Burovaya and Shorikha Formations of the Turukhansk Uplift. Data plotted include analyses of this study (circles and squares) as well as previously published data (Knoll et al., 1995; triangles). Section designations are the same as those given in Fig. 6.

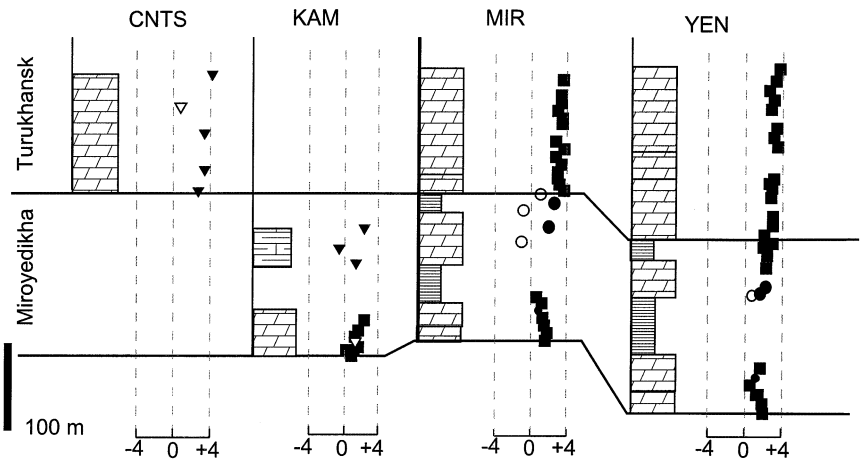

Fig. 8. Carbon isotope chemostratigraphy for the Miroyedikha and Turukhansk Formations of the Turukhansk Uplift. Data plotted include analyses of this study (circles and squares) as well as previously published data (Knoll et al., 1995; triangles). Symbols and section designations are same as Fig. 7 and Table 1.

Vinogradov, 1996) document maximum $\delta^{13}C$ values of $+6.0‰$ in the lower part of the Neryuen Formation and $+5.9‰$ in the uppermost Ignikan Formation. Very low sampling density in the Belaya River section precludes detailed comparison of the C isotopic profile in this section (Podkovyrov and Vinogradov, 1996) with that of the Maya River section (this study; Vinogradov et al., 1998). These very positive $\delta^{13}C$ values exceed the highest values previously reported for any Mesoproterozoic or early Neoproterozoic carbonates.

5.3. Strontium isotope chemostratigraphy

5.3.1. Turukhansk region

Of the seven carbonate-bearing Riphean Formations in the Turukhansk region, three formations (Linok, Sukhaya Tunguska, and Burovaya) yielded samples, which, judged by geochemical criteria, are very little altered and are therefore useful for reconstruction of the Sr isotopic composition of ancient seawater (Fig. 9, Tables 1 and 3). Combined with earlier datasets (Gorokhov et al., 1995), these data suggest that seawater $^{87}Sr/^{86}Sr$ values decrease smoothly from ~ 0.7060 in the Linok Formation to 0.7056 in best-preserved samples of the Sukhaya Tunguska Formation. Sr isotopic composition remains non-radiogenic, with lowest values near 0.7052 in the Burovaya Formation. Above the Burovaya Formation, minimum measured $^{87}Sr/^{86}Sr$ values are somewhat higher, near 0.7062, but must be considered to represent only a maximum constraint on coeval seawater.

Six samples from the Linok Formation were analyzed in this study. Three limestones were collected along the Nizhnyaya Tunguska River, from the central thrust-bounded block, and three along the Kammennaya River, from the same block. Samples from the Kammennaya River are moderately altered, according to geochemical criteria (Fig. 4) and show elevated $^{87}Sr/^{86}Sr$ values (0.70825–0.70959). Samples from the Nizhnyaya Tunguska River are well preserved and yield $^{87}Sr/^{86}Sr$ values between 0.70601 and 0.70697 (this study; Gorokhov et al., 1995). Analysis of seven little-altered samples from the hitherto unstudied sections of the Sukhaya Tunguska Formation, exposed along the Kammennaya and Sukhaya Tunguska Rivers, combined with four previously analyzed samples from the central Nizhnyaya Tunguska River section (Gorokhov et al., 1995) indicate that seawater $^{87}Sr/^{86}Sr$ was low through this interval. Samples from the lowermost, previously unstudied, part of the Sukhaya Tunguska Formation have $^{87}Sr/^{86}Sr$ values of 0.70590 and 0.70610. In the upper part of the formation, $^{87}Sr/^{86}Sr$ ratios are lower, with minimum measured values of 0.70532–0.70584 (this study; Gorokhov

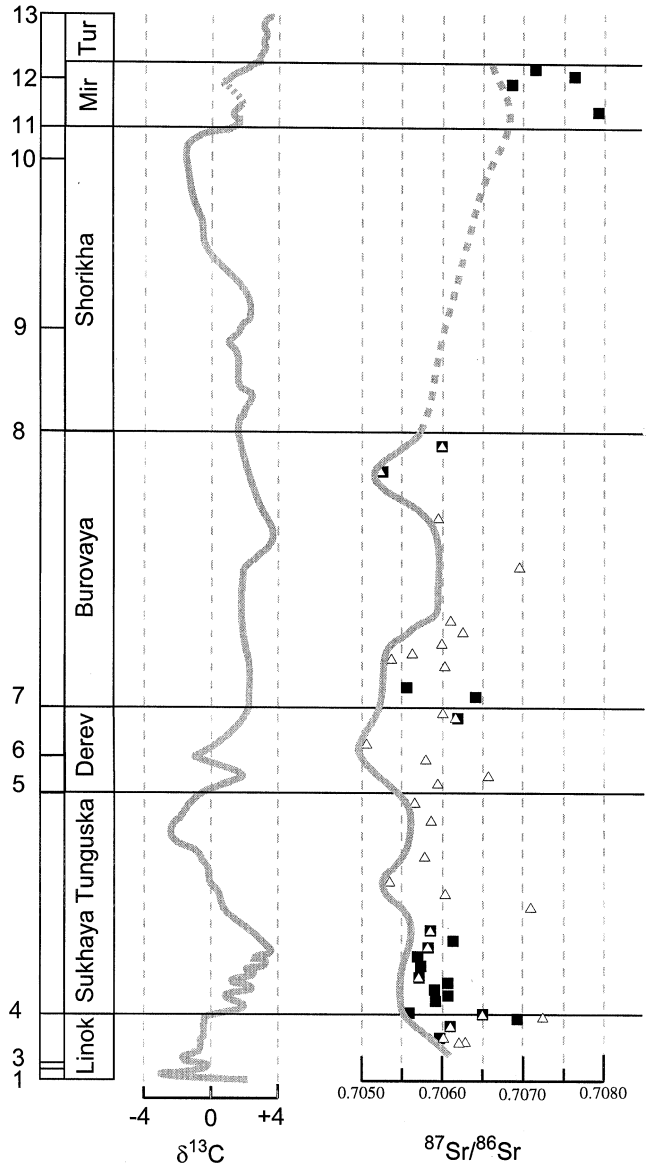

Fig. 9. Composite stratigraphic column with C and Sr isotope chemostratigraphy for the Turukhansk Uplift. Composite stratigraphic section was compiled using regionally correlated stratigraphic tie points. Tie points are as follows. 1 – base of Linok Formation; 2 – base of middle member of Linok Formation; 3 – top of middle member of Linok Formation; 4 – Linok/Sukhaya Tunguska contact; 5 – Sub-Derevnya unconformity; 6 – base of first shale in Derevnya Formation; 7 – Derevnya/Burovaya boundary; 8 – base of Shorikha Formation; 9 – *Minjaria* bioherm in Shorikha Formation; 10 – *Katavia* bioherm in Shorikha Formation; 11 – base of Miroyedikha Fm; 12 – top of lower shale in Miroyedikha Formation; 13 – top of Turukhansk Formation. Tie points were assigned where present in individual sections, and stratigraphic thicknesses were linearly interpolated between tie points. The consensus C isotopic curve represents a trace through the curve, with single outlying points omitted. Symbols for Sr isotopic composition are as follows: filled squares indicate data from this study; open triangles indicate data from Gorokhov et al. (1995). Note that the data of Gorokhov et al. (1995) have been age-corrected for Rb decay. Extremely radiogenic data (altered, $^{87}Sr/^{86}Sr > 0.7080$) in the Linok Formation were omitted from the graph (Table 1).

et al., 1995). Taken together, results from the Linok and Sukhaya Tunguska Formations support initial reports by Gorokhov et al. (1995) of a descending trend in $^{87}Sr/^{86}Sr$ from the Linok Formation through the Sukhaya Tunguska Formation (Table 3).

Carbonates, predominantly dolomitic, of the Derevnya Formation display a fairly wide range of variation in $^{87}Sr/^{86}Sr$, from 0.70584 to 0.70762 (Gorokhov et al., 1995; this study). Overall, these carbonates have high Mn/Sr ratios and poor textural preservation, and are likely diagenetically altered. Taking the lowest $^{87}Sr/^{86}Sr$ as most nearly approximating coeval seawater, the Derevnya carbonates are consistent with $^{87}Sr/^{86}Sr$ near 0.7058 (Gorokhov et al., 1995).

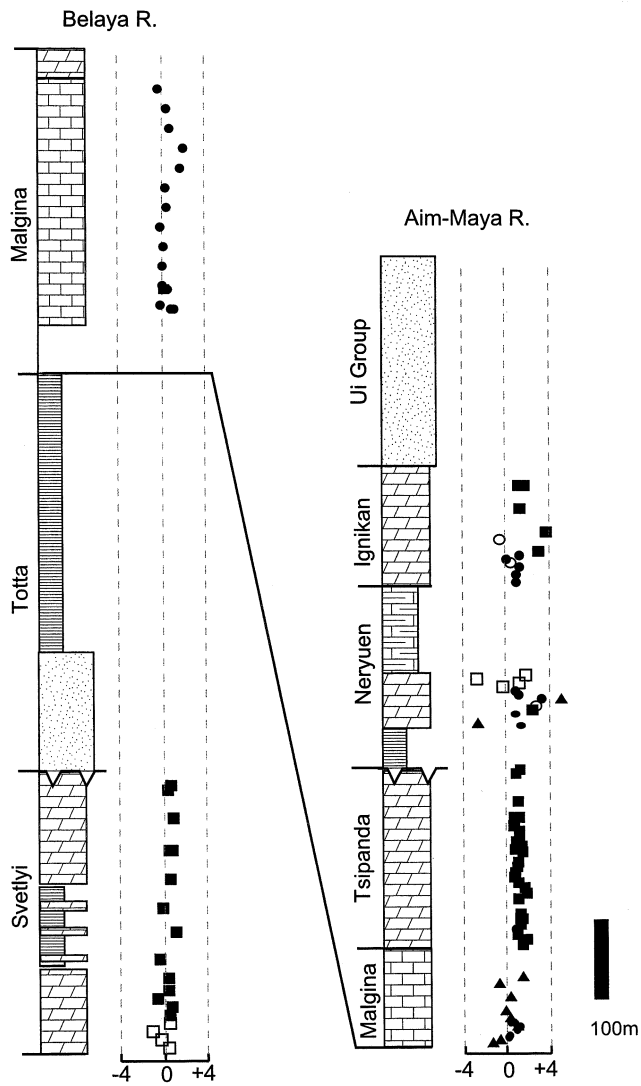

Fig. 10. Carbon isotope chemostratigraphy for the Uchur–Maya succession. Sampled parts of the successions from the Belaya and Aim–Maya Rivers are shown. Data plotted include analyses of this study (circles and squares) as well as previously published data (triangles, Vinogradov et al., 1998). See Fig. 7 for legend.

Table 3
Summary of C and Sr isotopic composition by formation in the Turukhansk region

Formation	Avg. $\delta^{13}C$	$\delta^{13}C$ range	$^{87}Sr/^{86}Sr_{min}$
Turukhansk	+3.1‰	From +2.1‰ to +4.2‰	0.70622
Miroyedikha	+1.5‰	From −0.4‰ to +2.5‰	0.70688
Shorikha	+0.8‰	From −5.0‰ to +4.0‰	NA
Burovaya	+2.3‰	From +0.3‰ to +4.6‰	0.70523
Derevnya	+0.7‰	From −5.5‰ to +2.6‰	0.70584
S. Tunguska	+0.5‰	From −2.7‰ to +3.3‰	0.70532
Linok	−0.7‰	From −2.2‰ to 2.2‰	0.70601

Only carbonates considered little altered by selection criteria (see text) are included in this table. This summary includes new data (this study) as well as previously published data (Gorokhov et al., 1995; Knoll et al., 1995). Figs. 6–9 plot data in stratigraphic context.

Burovaya Formation carbonates display a wide range of variation in both geochemical indicators of alteration (Fig. 4) and in $^{87}Sr/^{86}Sr$ ratios (Table 1), which range between 0.70523 and 0.70630 in limestones and 0.70592–0.70627 in dolostones (this study; Gorokhov et al., 1995). The least altered samples in this set give a minimum $^{87}Sr/^{86}Sr$ value of 0.70523 (Table 3).

Dolostones of the Shorikha Formation have been recrystallized in a medium with highly radiogenic Sr and are not suitable for evaluation of initial Sr isotopic composition. In general, limestones of the Miroyedikha Formation also display evidence of alteration. In order to place constraints on $^{87}Sr/^{86}Sr$ during Miroyedikha deposition, four samples with relatively low Mn/Sr ratios (1.09–6.19), high Sr content (56–341 ppm), and slightly depleted $\delta^{18}O$ values (from −7.7 to −9.6‰) were chosen. These best-preserved samples nonetheless yield relatively radiogenic $^{87}Sr/^{86}Sr$ values (0.70688–0.70793), compared to underlying units. Dolostones of the Turukhansk Formation had elevated Fe/Sr values and a minimum $^{87}Sr/^{86}Sr$ initial ratio of 0.70622 (Gorokhov et al., 1995). In light of the geochemical data it is most likely that the more radiogenic Sr isotopic compositions observed in carbonates of the Miroyedikha and Turukhansk Formations reflect diagenetic alteration of primary seawater Sr isotopic values, although the data leave room for the interpretation that an overall rise in seawater $^{87}Sr/^{86}Sr$ might have occurred during Miroyedikha and Turukhansk time.

5.3.2. Uchur–Maya region

In this region, seawater $^{87}Sr/^{86}Sr$ ratios are likely preserved only in carbonates of the lower Lakhanda Group. Limestones from the Malgina Formation and dolostones of the Tsipanda Formation yield a very broad range of Sr isotopic compositions, Mn/Sr ratios, and Fe/Sr ratios, indicating a complex diagenetic history (Fig. 5, Table 2). In an effort to reconstruct initial seawater $^{87}Sr/^{86}Sr$ values, 14 samples from the Malgina and Tsipanda Formations were evaluated for Sr isotopic composition. Samples were analyzed with and without pre-treatment with ammonium acetate, which removes the easily mobilized Sr from the carbonate prior to analysis (e.g., Gorokhov et al., 1995; Montañez et al., 1998). The $^{87}Sr/^{86}Sr$ ratios for Malgina limestones treated with ammonium acetate cluster near 0.70651 (Table 4), while untreated samples yielded $^{87}Sr/^{86}Sr$ ratios $\geqslant$ 0.70757. Tsipanda dolostones yield slightly more radiogenic ratios, with $^{87}Sr/^{86}Sr$ values of treated samples $\geqslant$0.70702, and untreated samples $\geqslant$ 0.70743. Recent data of Vinogradov et al. (1998) report lower initial $^{87}Sr/^{86}Sr$ ratios for petrographically and geochemically uncharacterized carbonates of the Malgina and Tsipanda Formations, sampled along the Maya River. A sample from the Malgina Formation, corrected for an age of 1100–1060 Ma, yielded an initial $^{87}Sr/^{86}Sr$ ratio of 0.70605 and two samples from the Tsipanda Formation yielded values of 0.70543 and 0.70588. It is likely that some enrichment in ^{87}Sr occurred in many of the Malgina carbonates as a consequence of circulation of diagenetic fluids through the underlying siliciclastic Totta Formation. Meteoric diagenesis associated with the sub-Lakhanda weathering surface would also be expected to contribute to alteration of the upper part of the Tsipanda Formation. These modes of exchange

have been reported in other successions, but are difficult to evaluate quantitatively (e.g., Mirota and Veizer, 1994; Gorokhov et al., 1995; Kuznetsov et al., 1997b).

Carbonates of the Lakhanda Group are better preserved than those of the Malgina and Tsipanda Formations. Four limestone samples from the middle carbonate unit of the Neryuen Formation along the Maya River exhibit low Mn/Sr ratios (0.2–1.3) and low (3.2–4.4) to slightly elevated (10.8–15.1) Fe/Sr ratios. The $^{87}Sr/^{86}Sr$ ratios of these carbonates lie between 0.70566 and 0.70577 (Fig. 11, Table 4). Two samples from the Maya River section of the Ignikan Formation, with slightly elevated Mn/Sr and Fe/Sr ratios, have $^{87}Sr/^{86}Sr$ values of 0.70576 and 0.70681.

These values are comparable to $^{87}Sr/^{86}Sr$ values of best-preserved Lakhanda Group carbonates from the Belaya River section in the northern part of the Yudoma–Maya Belt (Semikhatov et al., 1998a). Six little-altered limestones from the lower and middle parts of the Neryuen Formation along the Belaya River exhibit initial $^{87}Sr/^{86}Sr$ ratios between 0.70519 and 0.70554. These samples are exceptionally well preserved, with very low Mn/Sr (0.02–0.2) and Fe/Sr (0.1–5.0) ratios (Semikhatov et al., 1998a). Other samples from the Neryven Formation, as well as carbonates of the Ignikan Formation from this section are less well preserved and record more radiogenic and variable Sr isotopic compositions (0.70601–0.70784).

Table 4
Summary of C and Sr isotopic composition by formation in the Uchur–Maya region

Formation	Avg $\delta^{13}C$	$\delta^{13}C$ range	$^{87}Sr/^{86}Sr_{min}$
Ignikan	+1.4‰	From −0.1‰ to +3.6‰[a]	0.70576[a]
		Max 5.9‰[b]	0.70601[c]
Neryuen	+1.5‰	From −0.7‰ to +3.1‰[a]	0.70566[a]
		From −2.8‰ to +6.0‰[d]	0.70519[c]
Tsipanda	+1.0‰	From +0.5‰ to +1.7‰[a]	0.70702[a]
			0.70543[b]
Malgina	+0.3‰	From −0.5‰ to +1.9‰[a]	0.70651[a]
		From −1.9‰ to +0.9‰[d]	0.70605[b]
Svetlyi	+0.4‰	From −0.6‰ to +1.1‰[a]	0.73770[a]

Only carbonates considered little altered by selection criteria (see text) are included in this table. This summary includes new data (this study) as well as previously published data (Podkovyrov and Vinogradov, 1996; Semikhatov et al., 1998a; Vinogradov et al., 1998). Figs. 10 and 11 plot data in stratigraphic context.

[a] Data from this study.

[b] Data from Podkovyrov and Vinogradov (1996).

[c] Data from Semikhatov et al. (1998a,b).

[d] Data from Vinogradov et al. (1998).

6. Discussion

6.1. Correlation of the Turukhansk and Uchur–Maya regions

C and Sr chemostratigraphic data broadly corroborate present correlations suggested by lithology, biostratigraphy, and paleomagnetism, while at the same time providing an independent tool with which to refine correlations and connect Siberian successions to global geochemical events. The nearly invariant C isotopic profile of the Svetlyi Formation (from −0.6‰ to +1.1‰) differs from any unit in the Turukhansk succession, and suggests that the Svetlyi Formation is older than any carbonates of the Turukhansk Uplift. However, the observed pattern is similar to C isotopic profiles of Mesoproterozoic carbonates older than ca. 1300 Ma, including those from northwestern Siberia (Pokrovsky and Vinogradov, 1991; Buick et al., 1995; Knoll et al., 1995; Xiao et al., 1997; Kah et al., 1999). This observation supports an Early Middle Riphean (early Mesoproterozoic) age for the Svetlyi Formation.

Stratigraphic variation in $\delta^{13}C_{carb}$ from the Malgina Formation (Fig. 10, Tables 2 and 4) is similar to the pattern observed in Linok carbonates (Fig. 6, Tables 1 and 3); both vary between ca. −2‰ and +2‰, with secular change organized into two or three packages of increasing, then decreasing, $\delta^{13}C$. Thus, both the overall C isotopic composition and its stratigraphic pattern of variation in the Malgina and Linok Forma-

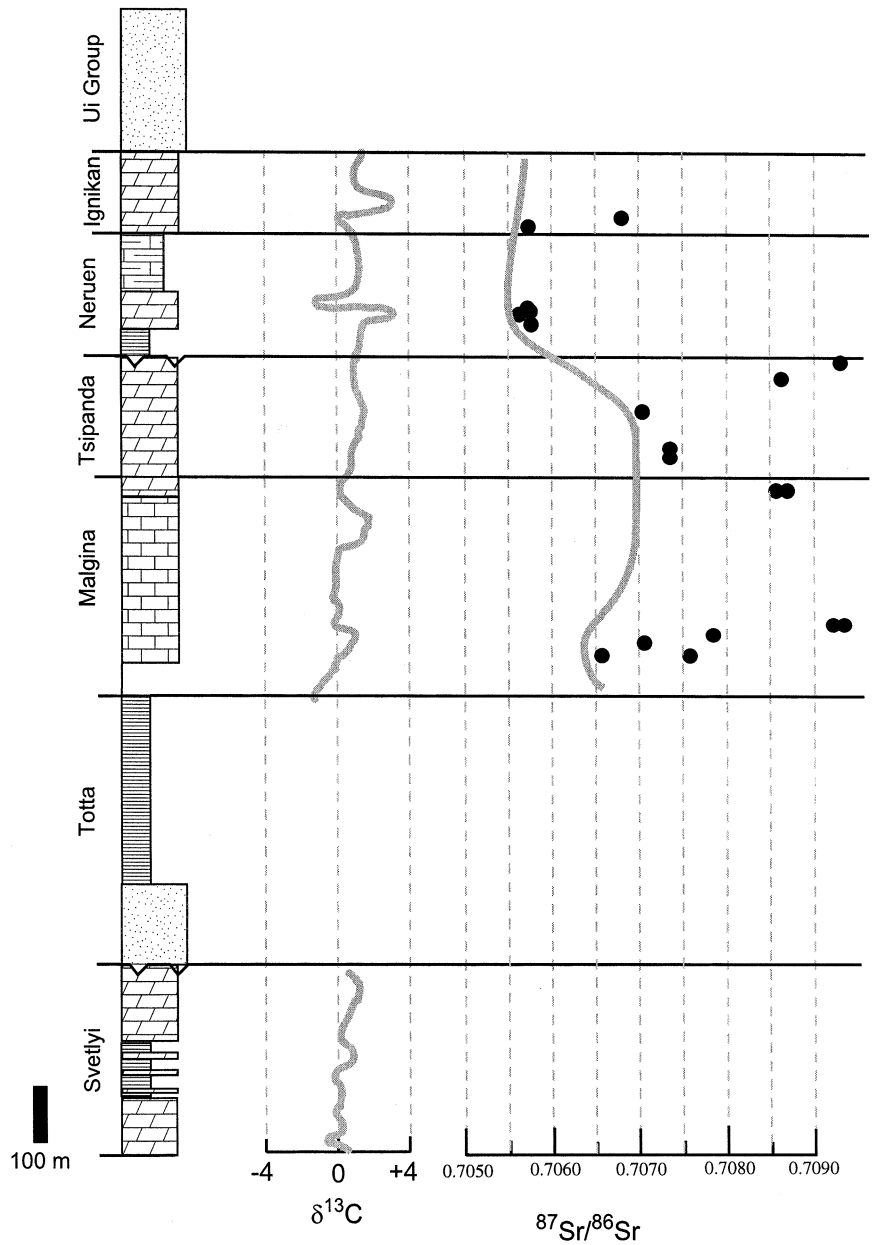

Fig. 11. Carbon and strontium isotope chemostratigraphy for the Uchur–Maya region, plotted on a composite stratigraphic column, showing the relative stratigraphic position of data from the sampled sections of the Riphean carbonates in the Uchur–Maya region (Yudoma–Maya Belt and Uchur–Maya Plate). Highly radiogenic data ($^{87}Sr/^{86}Sr > 0.7095$) are considered altered and were omitted from the graph (Table 2). See Fig. 7 for legend.

tions support other lines of evidence that suggest that these units are coeval.

In contrast, the Tsipanda and Sukhaya Tunguska Formations, which are traditionally regarded as coeval units, have very different C isotopic characteristics. Tsipanda carbonates record a narrow range of variation, between +0.5‰ and +1.7‰ (Fig. 10, Tables 2 and 4), whereas Sukhaya Tunguska carbonates show marked secular variation, organized as an oscillating rise from values near 0‰ to values of +3.3‰, followed by a drop to −2.7‰ and subsequent return to values near 0‰ (Fig. 6, Tables 1 and 3). Given that the correlation between the Malgina and Linok Formations appears secure, two explanations are possible. The first explanation suggests that C isotopic compositions in either the Sukhaya Tunguska Formation or the Tsipanda Formation might be diagenetically altered. This alternative is extremely unlikely for the Sukhaya Tunguska Formation, which displays excellent textural preservation, low Mn/Sr and Fe/Sr ratios, along with very non-radiogenic Sr isotopic values (Fig. 4). Likewise, although Tsipanda dolostones exhibit variability in geochemical indicators of diagenesis (Fig. 5) that urge caution in the interpretation of $^{87}Sr/^{86}Sr$ values, these alterations do not appear sufficient to obliterate an initial C isotopic signature: $\delta^{18}O$ values ($\bar{x} = 5.60‰$; $\sigma = 1.2‰$) do not indicate extensive exchange of O with diagenetic fluids, and $\delta^{13}C$ does not covary with $\delta^{18}O$; thus, it is difficult to support significant C exchange associated with diagenesis. The second explanation accepts the main trends in both successions as unaltered, and suggests that the traditional correlation (Fig. 3) be modified (Fig. 12). It is possible that Tsipanda deposition was concurrent with deposition of the upper Linok limestones, which represent an invariant isotopic interval and that most of the Sukhaya Tunguska Formation has no counterpart in the Uchur–Maya region. Such a correlation appears to be the most parsimonious from a chemostratigraphic standpoint and receives circumstantial support from a field-based conclusion that the Malgina–Tsipanda boundary is time transgressive (Semikhatov and Serebryakov, 1983). On the other hand, the Sukhaya Tunguska and Tsipanda Formations are sedimentologically similar, and direct evidence of a sub-Lakhanda unconformity, marked in the Uchur–Maya Plate sections, is not as pronounced in the Yudoma–Maya Belt. Unfortunately, the Sr isotopic data obtained in this and other studies do not allow an independent test of correlation hypotheses. Scattered Sr isotopic data reported by Vinogradov et al. (1998) indicate that minimum $^{87}Sr/^{86}Sr$ initial ratios recorded by the Malgina (0.70605) and Tsipanda (0.70543) are

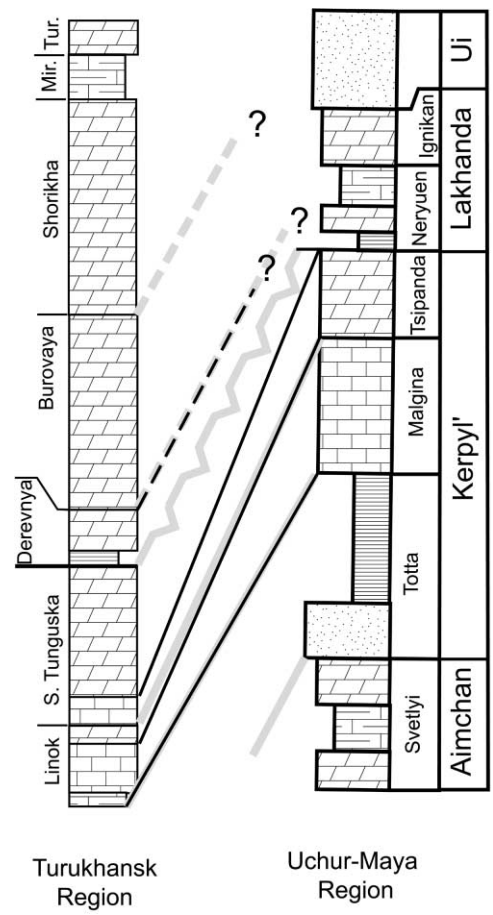

Fig. 12. Revised correlation for the Uchur–Maya and Turukhansk regions, based on new radiometric ages (Rainbird et al., 1997, 1998; Semikhatov et al., 2000; Khudoley et al., in press) and chemostratigraphic data (Gorokhov et al., 1995; Knoll et al., 1995; Podkovyrov and Vinogradov, 1996; Semikhatov et al., 1998a,b; Vinogradov et al., 1998; this study). Thick gray lines represent traditional correlation (Fig. 3; Semikhatov and Serebryakov, 1983). Black lines show revisions to initial hypothesis, based on chemostratigraphic data. In this correlation, the Sukhaya Tunguska has no counterpart in the Uchur–Maya region, and the Tsipanda Formation is likely coeval with the upper Linok Formation.

similar to those obtained for the Linok (0.70601) and Sukhaya Tunguska (0.70567) Formations (Gorokhov et al., 1995; this study); however, these data can constrain correlation hypotheses only if we can independently constrain, in some detail, seawater $^{87}Sr/^{86}Sr$ variation through this interval, and, thus far, we cannot.

Chemostratigraphic data also support, or at least do not reject, the traditional correlation of upper units in the two regions. Carbonates of the Derevnya and Burovaya Formations have, on average, moderately positive $\delta^{13}C$ values (from $+1.8‰$ to $+3.5‰$), with maximal values confined to the upper part of the Burovaya Formation and an individual sample from the Derevnya yielding a strongly negative value ($-2.4‰$). This sample appears to be well preserved, and likely records a short-lived isotopic excursion (Fig. 7). The C isotopic composition of Neryuen carbonates (Fig. 10, Tables 2 and 4) is broadly similar to that of the Derevnya and Burovaya Formations. Additionally, consideration of data from this study, in conjunction with recently published data (Podkovyrov and Vinogradov, 1996; Vinogradov et al., 1998) suggests a similar degree of variability.

The Lakhanda Group, however, evidently contains intervals with significantly more positive C isotopic compositions than does the Derevnya–Burovaya succession. C isotopic compositions as high as from $+5.0‰$ to $+6.0‰$ occur in the Neryuen Formation (Podkovyrov and Vinogradov, 1996; Vinogradov et al., 1998), and $\delta^{13}C$ values of $+5.9‰$ have been reported in carbonates near the top of the Ignikan Formation (Podkovyrov and Vinogradov, 1996). Although these samples cannot be placed precisely within a stratigraphic context, values as positive as these have not been observed in any other late Mesoproterozoic (earliest Upper Riphean) successions worldwide, and represent a distinctive anomaly in the emerging C isotopic record for this time interval.

Correlation of the Ignikan Formation and the uppermost Riphean units in the Turukhansk region is imprecise. Considering the diagenetic origin of the upper Shorikha negative C isotopic excursion (Knoll et al., 1995), the upper units from the Turukhansk succession exhibit two consecutive $\delta^{13}C$ trends from ca. $+2‰$ to moderately negative values in the Shorikha Formation and a subsequent rise in the Miroyedikha and Turukhansk Formations up to $+4.2‰$ at the top of the succession. Overall, $\delta^{13}C$ values of the Shorikha and Miroyedikha Formations are similar to those of the Ignikan Formation in the Uchur–Maya region (Tables 3 and 4), although individual events cannot be correlated. Overall, the Turukhansk Formation has more positive $\delta^{13}C$ values than the upper Lakhanda Group (Tables 3 and 4). The Sr isotopic data presently available for the Ignikan Formation and post-Burovaya part of the Turukhansk succession are obtained from altered samples and are unsuitable for chemostratigraphic interpretation.

The Sr isotopic compositions of the samples obtained from the Neryuen Formation compare closely with those of the Derevnya–Burovaya succession (Tables 3 and 4). Least-altered lower Lakhanda carbonates have slightly lower initial $^{87}Sr/^{86}Sr$ ratios (0.70519–0.70566; Semikhatov et al., 1998a,b; this study) than those of the Linok and upper Sukhaya Tunguska Formations (0.70611–0.70652 and 0.70567–0.70584, respectively), but ratios are virtually identical to those of the best-preserved samples from the Burovaya Formation (0.70523–0.70555; Gorokhov et al., 1995; this study). Taken together, these data indicate that non-radiogenic $^{87}Sr/^{86}Sr$ values characterized the oceans for a long interval that spanned the Middle–Upper Riphean boundary (Gorokhov et al., 1996a,b; Kuznetsov et al., 1997a; Semikhatov et al., 1998a,b), not just during a short-lived Neoproterozoic 'mantle event' (Veizer, 1983; Asmerom et al., 1991).

6.2. Implications for global events

The ultimate goal of chemostratigraphic study is to evaluate chemical and isotopic changes in the global ocean through time, and to correlate these changes with potential causal events. The data reported here, combined with data from previous studies, provide only a suggestion of the evolution of seawater during this interval of Earth history. As data accumulates from successions worldwide, our understanding of Mesoproterozoic seawater evolution improves, changing incrementally with each new dataset. The two, broadly coeval, regions of Siberia discussed in this paper can now be inter-

preted within the context of the broader Proterozoic record of C and Sr isotopic change. With an expanded data set, a pattern continues to emerge that links Proterozoic biogeochemistry with the major tectonic events of the time.

The C isotopic record of the post-2000 Ma Proterozoic can be conveniently subdivided into three parts (Kah et al., 1999). The first, comprising the Late Paleoproterozoic and early Mesoproterozoic (2000–1250 Ma), is characterized by C isotopic values near 0 ± 1‰, and records an unprecedented interval of long-term C isotopic stasis which began ca. 2000 Ma (Brasier and Lindsay, 1998). The second interval, addressed in this paper, spans the Mesoproterozoic–Neoproterozoic transition (from ~ 1250 to ~ 850 Ma) and is recognized by moderately positive average $\delta^{13}C$ values (up to $+4$‰, and rarely higher) and moderate variation in C isotopic composition. The third interval begins after 850 Ma and contains large, rapid variations in $\delta^{13}C$, with a generally elevated baseline ($\sim +5$‰; Kaufman and Knoll, 1995), observed in successions worldwide.

Evolution of carbonate $\delta^{13}C$ to more positive values reflects increased biomass and/or increased proportional burial of isotopically light organic matter, potentially attributable to one of several tectonic forcing mechanisms. First, high rates of organic C burial may be associated with increased continental margin length during periods of rifting, such as that observed during the Neoproterozoic break-up of Rodinia (Knoll, 1992; Hoffman, 1999). Periods of orogenesis, associated with high siliciclastic burial rates, may also result in increased organic C deposition (Derry et al., 1992; Des Marais, 1994, 1997a,b), although certain biotic events (e.g., expansion of cyanobacterial ecosystems) have been proposed to contribute to $\delta^{13}C$ rise as well (Semikhatov et al., 1999). The observed long-term changes in the character of the global C isotopic curve in the latter part of the Mesoproterozoic likely record long-term changes in the character of global biogeochemical cycling, and are plausibly linked to the assembly of the supercontinent Rodinia.

Secular change in Sr isotopic composition not only provides a second tool for correlating carbonate successions, but can also constrain interpretations of global tectonic processes. Because of the constant decay of ^{87}Rb in upper mantle rocks, there has been a long-term evolution of $^{87}Sr/^{86}Sr$ in the lithosphere from ~ 0.700 at 4000 Ma to ~ 0.703 at present (Veizer and Compston, 1976; Mirota and Veizer, 1994). For this reason, the Sr isotopic composition of hydrothermal input to the oceans has evolved toward higher values. Superimposed on this vectoral record of mantle and crustal aging are episodic variations in the flux of Sr from hydrothermal and continental sources to the oceans. These are associated with discrete episodes of rifting and orogeny (Raymo et al., 1988; Richter and Turekian, 1993). Both the magnitude and isotopic composition of this flux are dependent upon the nature and age of the continental crust that is exposed and eroded (Edmond, 1992). If the assembly of Rodinia is one of the primary factors affecting late Mesoproterozoic cycling of carbon, the Sr isotopic record of this time interval might be expected to shed light on reconstructing the relationship between tectonics and global geochemical cycles.

The geochemical record of the Late Paleoproterozoic to early Mesoproterozoic, which spans some 700 million years (2000–1300 Ma), is rather fragmentary; with intensified study, however, a pattern appears to be emerging. Overall, carbonate C isotopic values of this age are invariant and near 0‰ (Pokrovsky and Vinogradov, 1991; Buick et al., 1995; Knoll et al., 1995; Khabarov et al., 1996; Frank et al., 1997; Xiao et al., 1997; Brasier and Lindsay, 1998). Brasier and Lindsay (1998) attributed this stasis to general tectonic quiescence, but Sr isotopic data as well as geologic history call such an interpretation into question. Extensive orogenesis occurred during the Late Paleoproterozoic, as evidenced by the widespread and nearly coeval Svecofennian, Hudsonian, and Barramundi orogenies (Hoffman, 1988; Page, 1988; Plumb, 1990; Rosen et al., 1994), amalgamation of Laurentia between 1910 and 1630 Ma (Hoffman, 1988), and subsequent erosion of the resultant sutures. Between 1900 and 1600 Ma, $^{87}Sr/^{86}Sr$ ratios rise from ~ 0.7047 to ~ 0.7060 (Veizer et al., 1992; Whittaker et al., 1998). The earliest Mesoproterozoic (Lower Riphean) is marked by overall marine transgres-

sion, observed on several continents (Semikhatov, 1974; Ronov et al., 1984; Page, 1988; Semikhatov and Raaben, 1994; Page and Sweet, 1998) and by the onset of Lower Riphean rifting (Semikhatov, 1974; Ronov et al., 1984; Trompette, 1994). These events are coincident with a fall in $^{87}Sr/^{86}Sr$ between 1600 and 1400 Ma, from ~ 0.7060 to 0.7040 or lower (Veizer and Compston, 1976; Pokrovsky and Vinogradov, 1991; Veizer et al., 1992; Gorokhov et al., 1995). These geologic events and Sr isotope variations appear to be at odds with the observation of C isotopic stability. Brasier and Lindsay (1998) rightly stress the global significance of this C isotopic (non)event, but an explanation is perhaps more elusive than it first appeared.

Over the past few years, considerable progress has been made toward an improved understanding of C and Sr isotopic variations in late Mesoproterozoic and early Neoproterozoic seawater (ca. 1250–850 Ma). Based on Sr isotopic analyses of carbonates from this time interval in Siberia (Pokrovsky and Vinogradov, 1991; Gorokhov et al., 1995; Semikhatov et al., 1998a,b; Vinogradov et al., 1998; this study), the southern Urals (Gorokhov et al., 1996a,b; Kuznetsov et al., 1997a,b), and arctic Canada (Kah et al., 2001), it appears that $^{87}Sr/^{86}Sr$ in Late Mesoproterozoic seawater rose from early Mesoproterozoic lows (~ 0.7040) to values as high as 0.7060–0.7065 during deposition of the Linok and Malgina Formations (< 1300 Ma), while $\delta^{13}C$ values remained near 0‰. Following this interval, $^{87}Sr/^{86}Sr$ fell steadily, in carbonates of the Lakhanda Group (from ~ 1030 to > 1004 Ma) and the Sukhaya Tunguska (1035 ± 60 Ma) and Burovaya Formations, reaching values as low as 0.7051. At the same time, $\delta^{13}C$ values rose sharply to near $+3.5$‰, with variations of a few permil up to $+6$‰ (Knoll et al., 1995; Podkovyrov and Vinogradov, 1996; Vinogradov et al., 1998; Kah et al., 1999; 2001).

The onset of arc formation and arc-continent collisions at the margins of Laurentia began ca. 1300 Ma (McLelland et al., 1996), marking the beginnings of Rodinia assembly. The protracted assembly event ultimately resulted in continent–continent collision and the uplift of a global chain of mountain belts (Dalziel, 1991; Hoffman, 1991), which reached peak thermal metamorphism asynchronously over the interval 1160–1050 Ma (Mezger et al., 1991, 1993; McLelland et al., 1996; Cosca et al., 1998), and unroofing occurred nearly concurrently with peak thermal events (Cosca et al., 1991, 1992, 1998). Unroofing continued until 850–800 Ma at a uniformly low rate (Cosca et al., 1991; Mezger et al., 1991; Cosca et al., 1992; McLelland et al., 1996; Cosca et al., 1998).

Slightly elevated $^{87}Sr/^{86}Sr$ values recorded in the Linok and Malgina Formations relative to early Mesoproterozoic low values are consistent with an increased continental input of Sr to seawater and correspond broadly in time to early events associated with the initial stages in the assembly of Rodinia (McLelland et al., 1996). Curiously, however, seawater $^{87}Sr/^{86}Sr$ then displays a fall to non-radiogenic values that began by 1200 Ma (Kah et al., in press) and continues through the Middle–Upper Riphean boundary, recorded in the Sukhaya Tunguska, Burovaya, and Neryuen Formations. These results are inconsistent with an increased flux of radiogenic Sr during the latest Mesoproterozoic Ottowan orogeny and associated collisions. Rather, available data suggest one or both of the following possibilities: (1) the continental Sr flux in the late Mesoproterozoic was non-radiogenic due to the exhumation of predominantly juvenile crustal rocks; and (2) the hydrothermal flux increased due to increased mid-ocean ridge activity. Such activity might have produced the widespread Early Upper Riphean transgression (Semikhatov, 1974; Ronov et al., 1984; Semikhatov and Raaben, 1994, 1996), which, by itself could contribute to reduction of radiogenic Sr influx due to flooding of the source areas.

Elevated $^{87}Sr/^{86}Sr$ ratios exhibited by carbonates of the Ignikan, Miroyedikha, and Turukhansk Formations likely reflect diagenetic alteration, as suggested by geochemical criteria. In order to resolve global Sr-isotopic trends, we must look to other successions that preserve earliest Neoproterozoic carbonate rocks. The 970–

890 Ma Katav Formation of the Southern Urals displays similarly altered Sr isotopic (0.70608–0.71461) and trace elemental values (Gorokhov et al., 1996a,b; Kuznetsov et al., 1997a). However, by the time of deposition of the lower Inzer Formation in the Southern Urals (836 ± 27 Ma; Ovchinnikova et al., 1998), $^{87}Sr/^{86}Sr$ values are again low, between 0.70525 and 0.70538. Because earliest Neoproterozoic carbonates are not well-preserved, it is not presently possible to state with certainty whether the low Sr-isotopic values that characterize the latter half of the Mesoproterozoic (ca. 1200–1000 Ma) continue with little change through ca. 850–800 Ma, or whether the unroofing events of the terminal Mesoproterozoic are reflected in a rise in coeval seawater $^{87}Sr/^{86}Sr$ during the earliest Neoproterozoic.

Subsequent to this interval, the upper Inzer Formation and ca. 780 Ma Min'yar Formation (Ovchinnikova et al., 2000) of the Southern Urals record a well-preserved increase in $^{87}Sr/^{86}Sr$ from 0.70555 to 0.70611 (Kuznetsov et al., 1997a,b, 1998a). This increase in $^{87}Sr/^{86}Sr$ may be attributable to the Baikalian (850–860 Ma) and pre-Sinian Jenning (860–820 Ma) orogenies and related sea level fall (Gorokhov et al., 1995; Semikhatov et al., 1998a,b), which are widely documented in Siberia and on both the South China and North China platforms (see Semikhatov and Raaben, 1994; Khomentovsky, 1996; Semikhatov and Raaben, 1996 and references therein).

7. Conclusions

The purpose of chemostratigraphic analysis is fourfold: (1) to document secular isotopic variations in individual sedimentary successions on the basis of rigorous selection of least-altered samples; (2) to enable correlations among successions on a single continent; (3) by combining data from distant sequences, to begin to establish a global picture of geochemical change through a time interval; (4) to place global geochemical signatures into a geologic context, allowing interpretation of linkages among tectonics, geochemical cycling, and, ultimately, biotic events. The geochemical data from the Turukhansk and Uchur–Maya region speak to all four goals, albeit incompletely. Although not without significant complexity, the Siberian sections provide the most complete record of geochemical change to date through the late Mesoproterozoic and early Neoproterozoic, and the data discussed here contribute to an advancing global perspective for this time interval.

Regional C isotopic patterns are consistent with those articulated by Kah et al. (1999) for the Mesoproterozoic and early Neoproterozoic. Moderately positive C isotopic values, concomitant with modest secular variation, commence sometime after 1300 Ma and continue throughout the latest Mesoproterozoic and into the early Neoproterozoic. The Siberian Sr isotopic data (Gorokhov et al., 1995; Semikhatov et al., 1998a,b; Vinogradov et al., 1998; this study), combined with data from the Urals (Gorokhov et al., 1996a,b; Kuznetsov et al., 1997a,b, 1998a,b), and North America (Kah et al., in press) provide a record of the Sr isotopic composition of seawater during the assembly of Rodinia. In combination, the C and Sr isotopic data can be interpreted, albeit broadly, in terms of the major geologic events associated with Rodinia assembly. These data suggest that significant organic C production and burial occurred during early events, producing a significant first-order shift in global seawater $\delta^{13}C$ values. The lack of a distinctive, long-lived increase in $^{87}Sr/^{86}Sr$ during the late Mesoproterozoic suggests that significant juvenile crust was involved in mountain building, that relative hydrothermal flux from mid-ocean ridges remained high throughout the assembly of Rodinia and/or that increased continental runoff related to intense erosion of Grenvillian mountain belts terminated shortly after orogeny. Collectively, late Mesoproterozoic to early Neoproterozoic biological, biogeochemical, and tectonic events set in motion the coupled physical and biological changes that ultimately ushered in the Phanerozoic Eon.

Acknowledgements

We thank V.N. Sergeev and A.F. Veis for providing most of the samples from the Uchur–Maya region; O.V. Artemova for field and technical assistance in the course of preparation of this paper, B.G. Pokrovsky, I.M. Gorokhov, A.B. Kuznetsov, and L.C. Kah for helpful discussions and editorial advice. M. Saltzman and G. Shields provided thoughtful reviews that greatly improved the quality of the manuscript. Thanks to R. Walker for use of the TIMS facility at the University of Maryland. This research was supported in part by RFBR grant 99-05-64054 to MAS, by NASA exobiology grant NAG5-3654 to AHK, and by NSF grants EAR 96-30928 and EAR 96-14070 to Alan J. Kaufman.

References

Asmerom, Y., Jacobsen, S.B., Knoll, A.H., Butterfield, N.J., Swett, K., 1991. Strontium isotopic variations of Neoproterozoic seawater: implications for crustal evolution. Geochim. Cosmochim. Acta 55, 2883–2894.

Banner, J.L., 1995. Application of the trace element and isotope geochemistry of strontium to studies of carbonate diagenesis. Sedimentology 42, 805–824.

Banner, J.L., Hanson, G.N., 1990. Calculation of simultaneous isotopic and trace element variations during water-rock interaction with applications to carbonate diagenesis. Geochim. Cosmochim. Acta 54, 3123–3137.

Banner, J.L., Hanson, G.N., Meyers, W.J., 1988. Water-rock interaction history of regionally extensive dolomites of the Burlington–Keokuk Formation (Mississippian): isotopic evidence. In: Shukla, V., Baker, P. (Eds.), Sedimentology and Geochemistry of Dolostones, SEPM Special Publication, vol. 43. SEPM, Tulsa, pp. 97–114.

Berner, R.A., Canfield, D.E., 1989. A new model for atmospheric oxygen over Phanerozoic time. Am. J. Sci. 289, 333–361.

Bertrand-Sarfati, J., Moussine-Pouchkine, A., 1985. Evolution and environmental conditions of *Conophyton–Jacutophyton* associations in the Atar dolomite (Upper Proterozoic, Mauritania). Precambrian Res. 29, 207–234.

Brand, U., Veizer, J., 1980. Chemical diagenesis of a multicomponent carbonate system – 1. Trace elements. J. Sediment. Petrol. 50, 1219–1236.

Brasier, M.D., Lindsay, J.F., 1998. A billion years of environmental stability and the emergence of eukaryotes: new data from northern Australia. Geology 26, 555–558.

Brasier, M.D., Shields, G., Kuleshov, V.N., Zhegallo, L.A., 1996. Integrated chemo- and biostratigraphic calibration of early animal evolution: Neoproterozoic–early Cambrian of southwest Mongolia. Geol. Mag. 133, 445–485.

Buick, R., Des Marais, D.J., Knoll, A.H., 1995. Stable isotopic compositions of carbonates from the Mesoproterozoic Bangemall Group, northwestern Australia. Chem. Geol. 123, 153–171.

Butterfield, N.J., 2001. Paleobiology of the late Mesoproterozoic (ca. 1200 Ma) Hunting Formation, Somerset Island, arctic Canada. Precambrian Res. 111, 237–258.

Butterfield, N.J., Knoll, A.H., Swett, K., 1990. A bangiophyte red alga from the Proterozoic of Arctic Canada. Science 250, 104–107.

Canfield, D.E., 1999. A new model for Proterozoic ocean chemistry. Nature 396, 450–453.

Cosca, M.A., Sutter, J.F., Essene, E.J., 1991. Cooling and inferred uplift/erosion history of the Grenville Orogen, Ontario; constraints from $^{40}Ar/^{39}Ar$ thermochronology. Tectonics 10, 959–977.

Cosca, M.A., Essene, E.J., Kunk, M.J., Sutter, J.F., 1992. Differential unroofing within the Central Metasedimentary Belt of the Grenville Orogen; constraints from $^{40}Ar/^{39}Ar$ thermochronology. Contrib. Mineral. Petrol. 110, 211–225.

Cosca, M.A., Mezger, K., Essene, E.J., 1998. The Baltica–Laurentia connection; Sveconorwegian (Grenvillian) metamorphism, cooling, and unroofing in the Bamble Sector, Norway. J. Geol. 106, 539–552.

Dalziel, I.W.D., 1991. Pacific margins of Laurentia and East Antarctica–Australia as a conjugate rift pair: evidence and implications for an Eocambrian supercontinent. Geology 19, 598–601.

Derry, L.A., Kaufman, A.J., Jacobsen, S.B., 1992. Sedimentary cycling and environmental change in the Late Proterozoic: evidence from stable and radiogenic isotopes. Geochim. Cosmochim. Acta 56, 1317–1329.

Des Marais, D.J., 1994. Tectonic control of the crustal organic carbon reservoir during the Precambrian. Chem. Geol. 114, 303–314.

Des Marais, D.J., 1997a. Isotopic evolution of the biogeochemical carbon cycle during the Proterozoic Eon. Org. Geochem. 27, 185–193.

Des Marais, D.J., 1997b. Long-term evolution of the biogeochemical carbon cycle. In: Banfield, J.F., Nealson, K.H. (Eds.), Geomicrobiology; Interactions Between Microbes and Minerals, Reviews in Mineralogy, vol. 35. Mineralogical Society of America, Washington, DC, pp. 429–448.

Des Marais, D.J., Strauss, H., Summons, R.E., Hayes, J.M., 1992. Carbon isotope evidence for the stepwise oxidation of the Proterozoic environment. Nature 359, 605–609.

Edmond, J.M., 1992. Himalayan tectonics, weathering processes, and the strontium isotope record in marine limestones. Science 258, 1594–1597.

Fairchild, I.J., Marshall, J.D., Bertrand-Sarfati, J., 1990. Stratigraphic shifts in carbon isotopes from Proterozoic stromatolitic carbonates (Mauritania): influences of primary mineralogy and diagenesis. Am. J. Sci. 290-A, 46–79.

Frank, T.D., Lyons, T.W., Lohmann, K.C., 1997. Isotopic evidence for the paleoenvironmental evolution of the Mesoproterozoic Helena Formation, Belt Supergroup, Montana, USA. Geochim. Cosmochim. Acta 61, 5023–5041.

Gallet, Y., Pavlov, V.E., Semikhatov, M.A., Petrov, P.Y., 2000. Late Mesoproterozoic magnetostratigraphic results from Siberia: paleogeographic implications and magnetic field behaviour. J. Geophys. Res. B 105, 16481–16489.

German, T.N., 1981a. Filamentous algae from the Miroyedikha Formation of the upper Precambrian. Paleontol. J. 15, 111–116.

German, T.N., 1981b. Filamentous microorganisms in the Lakhanda Formation on the Maya River. Paleontol. J. 15, 100–107.

Gorokhov, I.M., 1996. Diagenez karbonatnykh osadkov: geokhimiya rasseyannykh elementov i isotopov strontziya (Diagenesis of carbonate deposits: trace element and Sr isotope behaviour). Lithologyya I Paleogeographiya 4, 141–164 in Russian.

Gorokhov, I.M., Semikhatov, M.A., Baskakov, A.V., Kutyavin, E.P., Mel'nikov, N.N., Sochava, A.V., Turchenko, T.L., 1995. Sr isotopic composition in Riphean, Vendian, and Lower Cambrian carbonates from Siberia. Stratigr. Geol. Correl. 3, 1–28.

Gorokhov, I.M., Semikhatov, M.A., Kuznetsov, A.B., Mel'nikov, N.N., 1996a. Improved reference curve of late Proterozoic seawater $^{87}Sr/^{86}Sr$. In: Bottrell, S.H., et al. (Eds.), Proceedings of the Fourth International Symposium on the Geochemistry of the Earth's Surface, Ilklen, Yorkshire. Leeds University Press, Uklen, Yorkshire, pp. 714–717.

Gorokhov, I.M., Semikhatov, M.A., Ovchinnikova, G.V., Kuznetsov, A.B., Mel'nikov, N.N., 1996b. Lead and strontium isotopes in ancient carbonates from the Urals and Siberia: evolution of seawater $^{87}Sr/^{86}Sr$ over the late Proterozoic. Goldschmidt Conf. J. of Conf. Abst. 1, 207.

Gorokhov, I.M., Mel'nikov, N.N., Turchenko, T.L., Kutyavin, E.P., 1997. Rb–Sr systematics of the pellite fraction of the early Riphean shales: Ust'll'ya Formation, Anabar Massif, Northern Siberia. Lithol. Min. Resour. 5, 530–539.

Hall, S.M., Veizer, J., 1996. Geochemistry of Precambrian carbonates: VII. Belt Supergroup, Montana and Idaho, USA. Geochim. Cosmochim. Acta 60, 667–677.

Hermann, T.N., 1990. Organicheskii Mir Milliard Let Nazad (The Organic World One Billion Years Ago). Nauka, Leningrad in Russian.

Hoffman, P.F., 1988. United plates of America, the birth of a craton; early Proterozoic assembly and growth of Laurentia. Annu. Rev. Earth Pl. Sci. 16, 543–603.

Hoffman, P.F., 1991. Did the breakout of Laurentia turn Gondwanaland inside-out? Science 252, 1409–1412.

Hoffman, P.F., 1999. The breakup of Rodinia, birth of Gondwana, true polar wander, and the snowball Earth. J. Afr. Earth Sci. 28, 9–26.

Hoffman, P.F., Kaufman, A.J., Halverson, G.P., 1998. Comings and goings of global glaciations on a Neoproterozoic tropical platform in Namibia. GSA Today 8, 1–9.

Jacobsen, S.B., Kaufman, A.J., 1999. The Sr, C and O isotopic evolution of Neoproterozoic seawater. Chem. Geol. 161, 37–57.

Jankauskas, T.V., Mikhailova, N.S., Hermann, T.N., Sergeev, V.N., et al., 1989. Mirofossilii dokembriya SSSR (Precambrian microfossils in the USSR). Nauka, Leningrad in Russian.

Kah, L.C., Sherman, A.B., Narbonne, G.M., Kaufman, A.J., Knoll, A.H., James, N.P., 1999. Isotope stratigraphy of the Mesoproterozoic Bylot Supergroup, Northern Baffin Island: implications for regional lithostratigraphic correlations. Can. J. Earth Sci. 36, 313–332.

Kah, L.C., Lyons, T.W. and Chesley, J.T., in press. Geochemistry of a 1.2 Ga carbonate-evaporite succession, northern Baffin and Bylot islands: implications for Mesoproterozoic marine evolution. Precambrian Res. 111, 203–236.

Kaufman, A.J., Knoll, A.H., 1995. Neoproterozoic variations in the C-isotopic composition of seawater: stratigraphic and biogeochemical implications. Precambrian Res. 73, 27–49.

Kaufman, A.J., Hayes, J.M., Knoll, A.H., Germs, G.J.B., 1991. Isotopic compositions of carbonates and organic carbon from upper Proterozoic successions in Namibia: stratigraphic variation and the effects of diagenesis and metamorphism. Precambrian Res. 49, 301–327.

Kaufman, A.J., Jacobsen, S.B., Knoll, A.H., 1993. The Vendian record of Sr and C isotopic variations in seawater: implications for tectonics and paleoclimate. Earth Pl. Sci. Lett. 120, 409–430.

Kaufman, A.J., Knoll, A.H., Narbonne, G.M., 1997. Isotopes, ice ages, and terminal Proterozoic Earth history. Proc. Natl. Acad. Sci. USA 94, 6600–6605.

Keller, B.M. (Ed.), 1982. Stratotip rifeya; paleontologiya paleomagnetizm (The Riphean stratotype; paleontology and paleomagnetism). Nauka, Moscow in Russian.

Khabarov, E.M., Tanygin, G.I., Morosova, I.P., Travin, A.N. and Nekhaev, A.Y., 1996. Isotopy ugleroda v karbonatakh zapada Sibirskoi platformy i evolutsiya isotopno-uglerodnoi sistemy v rifeiskikh basseinakh [Carbon isotopes in the carbonates of the western part of the Siberian Platform and C-isotope system evolution in the Riphean basins]. Geodinamika i evolutsiya Zemly. Abstr. Novosibirsk, p. 96–98 (in Russian).

Khomentovsky, V.V., 1996. Sinian system in China and its analogs in Siberia. Geol. Geophys. 37, 136–154.

Khudoley, A.K., Rainbird, R.H., Stern, R.A., Kropachev, A.P., Heaman, L.M., Zanin, A.M., Podkovyrov, V.N., Belova, V.N. and Sukhorukov, V.I., 2001. Sedimentary evolution of the Riphean-Vendian basin of southeastern Siberia. Precambrian Res. 111, 129–163.

Knoll, A.H., 1992. Biological and biogeochemical preludes to the Ediacaran radiation. In: Lipps, J.H., Signor, P.W. (Eds.), Origin and Early evolution of the Metazoa, Topics in Geobiology, vol. 10. Plenum, New York, pp. 53–84.

Knoll, A.H., Canfield, D.E., 1998. Isotopic inferences on early ecosystems. Paleontol. Soc. Pap. 4, 212–243.

Knoll, A.H., Semikhatov, M.A., 1998. The genesis and time distribution of two distinctive Proterozoic stromatolite microstructures. Palaios 13, 408–422.

Knoll, A.H., Sergeev, V.N., 1995. Taphonomic and evolutionary changes across the Mesoproterozoic–Neoproterozoic transition. Neues Jb. Geolog. Paläontol. Abh. 195, 289–302.

Knoll, A.H., Kaufman, A.J., Semikhatov, M.A., 1995. The carbon isotopic composition of Proterozoic carbonates: Riphean successions from northwestern Siberia (Anabar Massif, Turukhansk uplift). Am. J. Sci. 295, 823–850.

Komar, V.A., Semikhatov, M.A., Serebryakov, S.N., 1978. A stratigraphic scale for the Riphean deposits of the Uchur–Maya region. Internat. Geol. Rev. 20, 743–756.

Kuznetsov, A.B., Gorokhov, I.M., Mel'nikov, N.N., Konstantinova, G.V., Kutyavin, E.P., Turchenko, T.L., Kozlov, V.I., 1997a. Isotopnye rasnovidnosty Sr v izvestnyakakh karatavskoy serii, Yuzhnyi Ural (Sr isotope variation in the limestones of the Karatau Group, Southern Urals). In: Koroteev, V.A., Semikhatov, M.A., Maslov, A.V., et al. (Eds.), Riphean of Northern Eurasia. Geology and General Problems of Stratigraphy. Uralian Branch, Russian Academy of Sciences, Ekaterinburg, pp. 182–186 (in Russian).

Kuznetsov, A.B., Gorokhov, I.M., Semikhatov, M.A., Mel'nikov, N.N., Kozlov, V.I., 1997b. Strontium isotopic composition in the limestones of the Inzer Formation, Upper Riphean type section, Southern Urals. Trans. Russ. Acad. Sci./Earth Sci. 353, 319–324.

Kuznetsov, A.B., Gorokhov, I.M., Mel'nikov, N.N., Konstantinova, G.V., Kutyavin, E.P., Turchenko, T.L., 1998a. Dolomitizatsiya verkhnerifeiskikh karbonatov min'yarskoi svity, karatavskaya seriya, Yuzhnyi Ural (Dolomitization of the Upper Riphean carbonates of the Min'yar Formation, Karatau Group, Southern Urals). In: Shemyakin, V.M., Filippov, N.B., et al. (Eds.), Sedimentary Formations of the Precambrian and their Ore Deposits. Abstracts, Institute of Precambrian Geology and Geochronology. Russian Academy of Sciences, St. Petersburg, pp. 30–31 (in Russian).

Kuznetsov, A.B., Gorokhov, I.M., Semikhatov, M.A., Mel'nikov, N.N., Konstantinova, G.V., 1998b. Otnoshenie $^{87}Sr/^{86}Sr$ v morskoy vode v kontse pozdnego rifeya: karbonaty ukskoi svity, Yuzhnyi Ural ($^{87}Sr/^{86}Sr$ ratios in late Riphean seawater: Limestones of the Uk Formation, Southern Urals). In: Shemyakin, V.M., Filippov, N.B. (Eds.), Sedimentary Formations of the Precambrian and their Ore Deposits. Abstracts, Institute of Precambrian Geology and Geochronology. Russian Academy of Sciences, St. Petersburg, pp. 31–32 (in Russian).

Larin, A.M., Amelin, Y.V., Neymark, L.A., Krimsky, R.S., 1997. The origin of the 1.72–1.73 Ga anorogenic Ulkan volcano-plutonic complex, Siberian Platform, Russia: inferences from geochronological, geochemical, and Nd–Sr–Pb isotopic data. An. Acad. Bras. Cienc. 63, 295–312.

Lea, D.W., Martin, P.A., 1996. A rapid mass spectrometric method for the simultaneous analysis of barium, cadmium, and strontium in foraminifera shells. Geochim. Cosmochim. Acta 60, 3143–3149.

McLelland, J., Daly, J.S., McLelland, J.M., 1996. The Grenville orogenic cycle (ca. 1350–1000 Ma); an Adirondack perspective. Tectonophysics 265, 1–28.

McMenamin, M.A.S., McMenamin, D.L.S., 1990. The emergence of animals; the Cambrian breakthrough. Columbia University Press, New York.

Mezger, K., Rawnsley, C.M., Bohel, S.R., Hanson, G.H., 1991. U–Pb garnet, sphene, monazite, and rutile ages: implications for the duration of high-grade metamorphism and cooling histories, Adirondak Mountains, New York. J. Geol. 99, 415–428.

Mezger, K., Essene, E.J., van der Pluijm, B.A., Halliday, A.N., 1993. U–Pb geochronology of the Grenville Orogen in Ontario and New York: constraints on ancient crustal tectonics. Contrib. Mineral. Petrol. 114, 13–26.

Mirota, M.D., Veizer, J., 1994. Geochemistry of Precambrian carbonates: VI. Aphebian Albanel Formations, Quebec, Canada. Geochim. Cosmochim. Acta 58, 1735–1745.

Montañez, I.P., Osleger, D.A., Banner, J.L., Mack, L., Musgrove, M., 1998. Temporal extension of the newly resolved Middle to Late Cambrian seawater Sr isotope curve, southern Canadian Rockies and the Great Basin, USA. Amer. Assoc. Petr. Geol. Ann. Mtg. Abst. 1998, 517.

Neymark, L.A., Larin, A.M., Yakovleva, S.A., Gorokhovsky, B.M., 1992. Uranium–lead age of igneous rocks in the Ulkan graben in the southeastern part of the Aldan Shield. Trans. Russ. Acad. Sci./Earth Sci. 324, 92–96.

Nutman, A.P., Chernyshev, I.V., Baadsgaard, H., Smelov, A.P., 1992. The Aldan Shield of Siberia, USSR; the age of its Archaean components and evidence for widespread reworking in the mid-Proterozoic. Precambrian Res. 54, 195–210.

Nuzhnov, S.V., Yarmolyuk, V.A., 1959. Pozdnii dokembrii Yugo-vostochnoi okrainy Sibirskoi platformy (Late Precambrian of the south-eastern margin of the Siberian Platform). Sovetskaya geologiya 7, 21–31 (in Russian).

Ovchinnikova, G.V., Semikhatov, M.A., Gorokhov, I.M., Belyatskii, B.V., Vasilieva, I.M., Levskii, L.K., 1995. U–Pb systematics of Pre-Cambrian carbonates: the Riphean Sukhaya Tunguska Formation in the Turukhansk Uplift, Siberia. Lithology Min. Resour. 30, 525–536.

Ovchinnikova, G.V., Vasil'eva, I.M., Semikhatov, M.A., Kuznetsov, A.B., Gorokhov, I.M., Gorokhovskii, B.M., Levskii, L.K., 1998. U–Pb systematics of Proterozoic carbonate rocks: the Inzer Formation of the Upper Riphean stratotype (Southern Urals). Stratigr. Geol. Correl. 6, 336–347.

Ovchinnikova, G.V., Vasil'eva, I.M., Semikhatov, M.A., Gorokhov, I.M., Kuznetsov, A.B., Gorokhovskii, B.M., Levskii, L.K., 2000. Possibilities of Pb–Pb dating of carbonate rocks with distributed U–Pb systems: the Min'yar Formation of the Upper Riphean stratotype, South Urals. Stratigr. Geol. Correl. 8, 526–542.

Page, R.W., 1988. Geochronology of early to middle Proterozoic fold belts in northern Australia: a review. Precambrian Res. 40/41, 1–20.

Page, R.W., Sweet, I.P., 1998. Geochronology of basin phases in the western Mt. Isa Inlier, and correlation with the McArthur Basin. Aust. J. Earth Sci. 45, 219–232.

Pavlov, V.E., Petrov, P.Yu., 1996. Paleomagnitoe isucheniye rifeiskikh otlozhenii Turukhanskogo raiona (Paleomagnetic investigation of the Riphean sediments of the Turukhan region). Fiz. Zemli 3, 70–81 in Russian.

Pavlov, V.E., Burakov, K.S., Tselmovich, V.A., Zhuravlev, D.Z., 1992. Paleomagnetism sillov Uchuro–Maiskogo raiona I otsenka napryazhennosti geomagnitnogo polya v pozdnem rifee (Paleomagnetic characteristics of the Uchur–Maya region sills and evaluation of the Late Riphean geomagnetic field intensity). Fiz. Zemli 1, 92–101 in Russian.

Petrov, P.Y., 1993a. Depositional environments of the lower formations of the Riphean sequence, northern part of the Turukhansk Uplift, Siberia. Stratigr. Geol. Correl. 1, 181–191.

Petrov, P.Y., 1993b. Structure and sedimentation environments of the Riphean Bezymyannyi Formation in the Turukhansk Uplift, Siberia. Stratigr. Geol. Correl. 1, 490–502.

Petrov, P.Y., Semikhatov, M.A., 1997. Structure and environmental conditions of a transgressive Upper Riphean complex: Miroedikha Formation of the Turukhansk Uplift, Siberia. Lithology Min. Resour. 32, 11–29.

Petrov, P.Y., Semikhatov, M.A., 1998. The upper Riphean stromatolitic reefal complex; Burovaya Formation of the Turukhansk region, Siberia. Lithology Min. Resour. 33, 539–560.

Petrov, P.Y. and Semikhatov, M.A., 2001. Sequence organization and growth patterns of late Mesoproterozoic stromatolite reefs: an example from the Burovaya Formation, Turukhansk Uplift, Siberia. Precambrian Res. 111, 259–283.

Petrov, P.Y., Veis, A.F., 1995. Facial-ecological structure of the Derevnya Formation microbiota: Upper Riphean, Turukhansk Uplift, Siberia. Stratigr. Geol. Correl. 3, 435–460.

Petrov, P.Y., Semikhatov, M.A., Sergeev, V.N., 1995. Development of the Riphean carbonate platform and distribution of silicified microfossils: the Sukhaya Tunguska Formation, Turukhansk Uplift, Siberia. Stratigr. Geol. Correl. 3, 602–620.

Plumb, K.A., 1990. A new Precambrian time scale. Bulletin of Liaison and Informations, IGCP Project 196, Calibration of the Phanerozoic Time Scale, 8, 34–36.

Podkovyrov, V.N., Vinogradov, D.P., 1996. Epigenesis and preservation of carbon and oxygen isotope systems in the Upper Riphean-Vendian carbonates, the Lakhanda and Yudoma Groups, Belaya River sections, southeastern Yakutia. Lithology Min. Resour. 31, 483–492.

Podkovyrov, V.N., Semikhatov, M.A., Kuznetsov, A.B., Vinogradov, D.P., Kozlov, V.I., Kislova, I.V., 1998. Carbonate carbon isotopic composition in the Upper Riphean Stratotype, the Karatau Group, Southern Urals. Stratigr. Geol. Correl. 6, 319–335.

Pokrovsky, B.G., Vinogradov, V.I., 1991. Isotopnyi sostav strontsiya, kisloroda i ugleroda v verkhnedokembriyskikh karbonatakh zapadnogo sklona anabarskogo podnyatiya (reka Kotuikan) (Isotopic composition of strontium, oxygen, and carbon in the Upper Precambrian carbonates of the western slope of the Anabar Uplift (Kotuikan River)). Dokl. Akad. Nauk SSSR 320, 1245–1250 in Russian.

Powell, C.McA., Li, Z.X., Meert, J.G., Park, J.K., 1993. Paleomagnetic constraints on timing of the Neoproterozoic breakup of Rodinia and the Cambrian formation of Gondwana. Geology 21, 889–892.

Pyatiletov, V.G., 1988. Mikrofitofossilii pozdnego dokembriya Uchuro–Maiskogo raiona (Late Precambrian microphytofossils from the Uchur–Maya region). In: Khomentovsky, V.V. (Eds.), Pozdnii Dokembrii I rannii Paleozoi Sibiri. Rifei i Vend. Russian Academy of Sciences, Novosibirsk, pp. 47–104.

Rainbird, R.H., Stern, R.A., Khudoley, A.K., Kropachev, A.P., 1997. U–Pb detrital zircon geochronology and provenance of Riphean sedimentary rocks from SE Siberia; constraints for the Siberia–Laurentia connection. Geol. Soc. Am. Abstr. Prog. 29, 196–197.

Rainbird, R.H., Stern, R.A., Khudoley, A.K., Kropachev, A.P., Heaman, L.M., Sukhorukov, V.I., 1998. U–Pb geochronology of Riphean sandstone and gabbro from southeast Siberia and its bearing on the Laurentia–Siberia connection. Earth Pl. Sci. Lett. 164, 409–420.

Raymo, M.E., Ruddiman, W.F., Froelich, P.N., 1988. Influence of late Cenozoic mountain building on ocean geochemical cycles. Geology 16, 649–653.

Richter, F.M., Turekian, K.K., 1993. Simple models for the geochemical response of the ocean to climatic and tectonic forcing. Earth Pl. Sci. Lett. 119, 121–131.

Ronov, A.B., Khain, V.E. and Seslavinsky, K.B., 1984. Atlas litologo paleogeographicheskikh kart mira. Posdnii dokembrii i paleozoi kontinentov (Atlas of lithological-paleogeographical maps of the World. Late Precambrian and Paleozoic of continents), Leningrad (in Russian).

Rosen, O.M., Condie, K.C., Natapov, L.M., Nozhkin, A.D., 1994. Archean and early Proterozoic evolution of the Siberian Craton; a preliminary assessment. In: Condie, K.C. (Ed.), Archean Crustal Evolution, Developments in Precambrian Geology, vol. 11. Elsevier, Amsterdam, pp. 411–459.

Semikhatov, M.A., 1962. Rifei i niznii kembrii Yeniseiskogo kryazha (Riphean and Lower Cambrian of the Yenisei Ridge). Trudy, Geologicheskogo Instituta, Akademii Nauk SSSR, 68. Nauka, Moscow (in Russian).

Semikhatov, M.A., 1974. Stratigrafiya i geokhronologiya proterozoya (Proterozoic stratigraphy and geochronology). Nauka, Moscow in Russian.

Semikhatov, M.A., 1991. General problems of Proterozoic stratigraphy in the USSR. Sov. Scient. Rev. Geol. Sec. 1, 1–192.

Semikhatov, M.A., 1995. Methodic principles of the Riphean stratigraphy. Stratigr. Geol. Correl. 3, 559–574.

Semikhatov, M.A., Raaben, M.E., 1994. Dynamics of global diversity of Proterozoic stromatolites; Article 1, Northern Eurasia, China and India. Stratigr. Geol. Correl. 2, 492–513.

Semikhatov, M.A., Raaben, M.E., 1996. Dynamics of the global diversity of Proterozoic stromatolites; Article 2, Africa, Australia, North America and a general synthesis. Stratigr. Geol. Correl. 4, 492–513.

Semikhatov, M.A. and Serebryakov, S.N., 1978. Nizhniy rifey Sibirskoy platformy (Lower Riphean of the Siberian Platform). Trudy geologicheskogo Instituta, Akademii Nauk SSSR, Moscow, 312: 43–66 (in Russian).

Semikhatov, M.A. and Serebryakov, S.N., 1983. Sibirskii gipostratotip rifeya (The Siberian Hypostratotype of the Riphean). Trudy, Geologicheskogo Instituta, Akademii Nauk SSSR, 367. Nauka, Moscow (in Russian).

Semikhatov, M.A., Shurkin, K.A., Aksenov, E.M., Bekker, Y.R., Bobikova, E.V., Duk, V.L., Esipchuk, K.E., Karsakov, L.P., Kiselev, V.V., Kozlov, V.I., Lobach-Zhuchenko, S.B., Negrutsa, V.Z., Robonen, V.I., Sez'ko, A.I., Filatova, L.I., Khomentovsky, V.V., Shemyakin, V.M., Shuldiner, V.I., 1991. New stratigraphic scale for the Precambrian of the USSR. Izvestiya Akademii Nauk SSSR. Seriya Geologicheskaya 1991, 3–16.

Semikhatov, M.A., Gorokhov, I.M., Kuznetsov, A.B., Mel'nikov, N.N., Podkovyrov, V.N., Kislova, I.V., 1998a. The strontium isotopic composition in early Late Riphean seawater: limestones of the Lakhanda Group, the Uchur–Maya region, Siberia. Trans. Russ. Acad. Sci./Earth Sci. 360, 236–240.

Semikhatov, M.A., Kuznetsov, A.B., Gorokhov, I.M., Mel'nikov, N.N., Podkovyrov, V.N., Kutyavin, E.P., 1998b. Preobladanie mantiinogo Sr v morskoi vode nachala pozdnego rifeya: kratkovremennoe sobytie ili ustoichivaya tendentsiya? (Predominance of mantle Sr in the early Later Riphean seawater: a short-term episode or persistent trend?). In: Shemyakin, V.M., Fillipov, N.B. (Eds.), Sedimentary Formations of the Precambrian and their Ore Deposits. Abstracts, Institute of Precambrian Geology and Geochronology. Russian Academy of Sciences, St. Petersburg, pp. 65–66 (in Russian).

Semikhatov, M.A., Raaben, M.E., Sergeev, V.N., Veis, A.F., Artemova, O.V., 1999. Biotic events and positive $\delta^{13}C_{carb}$ anomaly at 2.3–2.06 Ga. Stratigr. Geol. Correl. 7, 413–436.

Semikhatov, M.A., Ovchinnikova, G.V., Gorokhov, I.M., Kuznetsov, A.B., Vasil'eva, I.M., Gorokhovskii, B.M., Podkovyrov, V.N., 2000. Isotopic age of the Middle–Upper Riphean boundary: Pb–Pb geochronology of the Lakhanda Group carbonates, Eastern Siberia. Trans. Russ. Acad. Sci./Earth Sci. 372, 216–221.

Serebryakov, S.N., 1975. Osobennosti formirovaniya i razhmetshiniya rifeiskikh stromatolitov Sibiri (Peculiarities of formation and location of the Riphean stromatolites in Siberia). Nauka, Moscow in Russian.

Serebryakov, S.N., 1976. Peculiarities of formation and distribution of Riphean stromatolites. In: Walter, M.R. (Ed.), Stromatolites. Elsevier, Amsterdam, pp. 321–336.

Sergeev, V.N., 1999. Silicified microfossils from the transitional Meso–Neoproterozoic deposits of the Turukhansk Uplift, Siberia. Societa Paleontol. Ital. Bull. Spec. Issue 38, 287–295.

Sergeev, V.N., Knoll, A.H., Grotzinger, J.P., 1995. Paleobiology of the Mesoproterozoic Billyakh Group, Anabar Uplift, Northern Siberia. J. Paleontol. Memoir 39, 1–37.

Sergeev, V.N., Knoll, A.H., Petrov, P.Y., 1997. Paleobiology of the Mesoproterozoic–Neoproterozoic transition: the Sukhaya Tunguska Formation, Turukhansk Uplift, Siberia. Precambrian Res. 85, 201–239.

Sharma, T., Clayton, R.N., 1965. Measurement of O-18/O-16 ratios of total oxygen of carbonates. Geochim. Cosmochim. Acta 29, 1347–1353.

Shenfil', V.Y., 1991. Pozdniy dokembriy Sibirskoy Platformy (The Late Precambrian of the Siberian Platform). Izd. Nauka, Novosibirsk (in Russian).

Smethurst, M.A., Khramov, A.N., Torsvik, T.H., 1998. The Neoproterozoic and Palaeozoic palaeomagnetic data for the Siberian Platform: from Rodinia to Pangea. Earth Sci. Rev. 43, 1–24.

Strauss, H., 1997. The isotopic composition of sedimentary sulfur through time. Palaeogeog. Palaeoclimat. Palaeoecol. 132, 97–118.

Trompette, R., 1994. Geology of Western Gondwana (2000–500 Ma). Pan-African-Brasiliano aggregation of South America and Africa. Balkema, Rotterdam.

Veis, A.F., 1988. Mikrofossilii v stratigrafii rifeya i venda Uchuro–Maiskogo i Turukhanskogo regionov Sibiri (Microfossils in the Riphean and Vendian stratigraphy of the Uchuro–Maya and Turukhansk regions of Siberia). Izvestiya Akademii Nauk SSSR, Seriya Geologicheskaya 5, 47–64 in Russian.

Veis, A.F., Petrov, P.Y., 1994. The main peculiarities of the environmental distribution of microfossils in the Riphean basins of Siberia. Stratigr. Geol. Correl. 2, 97–129.

Veis, A.F., Semikhatov, M.A., 1989. Nizhnerifeiskaya omakhtinskaya assotsiatsiya mikrofossilii Vostochnoi Sibiri: sostav i usloviya formirovaniya (Lower Riphean Omakhta assemblage of microfossils from eastern Siberia: composition and environments of formation). Izvestiya Akademii Nauk SSSR, Seriya Geologicheskaya 1989, 36–55 in Russian.

Veis, A.F., Vorob'eva, N.G., 1992. Mikrofossilii rifeya i venda Anabarskogo massiva (Riphean and Vendian microfossils of the Anabar Uplift). Izvest. RAN, Ser. Geolog. 1, 114–130 in Russian.

Veis, A.F., Petrov, P.Y., Vorob'eva, N.G., 1998a. The Late Riphean Miroedikha microbiota from Siberia. Part 1: composition and facial-ecological distribution of organic-walled microfossils. Stratigr. Geol. Correl. 6, 440–461.

Veis, A.F., Petrov, P.Y., Vorob'eva, N.G., 1998b. Secular transformations in the facial-ecological structure of Precambrian biotas and the Riphean stratigraphy. Geologiya i Geofizika 39, 85–96.

Veis, A.F., Petrov, P.Y., Vorob'eva, N.G., 1999. The Late Riphean Miroedikha microbiota from Siberia. Part 2: interpretation in terms of biotic paleosuccession. Stratigr. Geol. Correl. 7, 15–34.

Veis, A.F., Larionov, N.N., Vorob'eva, N.G., Li S-Jo, 2000. Microfossils and the Riphean stratigraphy, south Urals (Bashkir meganticlinorium) and Cis-Uralian region (Kama-Belaya aulocogene). Stratigr. Geol. Correl., 8, 415–432.

Veizer, J., 1983. Chemical diagenesis of carbonates: theory and application. In: Arthur, M.A., Anderson, T.F., Kaplan, I.R., Veizer, J. (Eds.), Stable Isotopes in Sedimentary Geology, SEPM Short Course, vol. 10. SEPM, Tulsa, pp. 3-1–3-100.

Veizer, J., Compston, W., 1976. $^{87}Sr/^{86}Sr$ in Precambrian carbonates as an index of crustal evolution. Geochim. Cosmochim. Acta 40, 905–914.

Veizer, J., Clayton, R.N., Hinton, R.W., 1992. Geochemistry of Precambrian carbonates: IV. Early Paleoproterozoic (2.25 ± 0.25 Ga) seawater. Geochim. Cosmochim. Acta 56, 875–885.

Vinogradov, V.I., Pokrovsky, B.G., Golovin, D.I., Bujakaite, M.I., Murav'ev, V.I., Veis, A.F., 1998. Isotopic evidences of epigenetic transformations and the problem of the age of Riphean rocks in the Uchur–Maya region, Eastern Siberia. Lithology Min. Resour. 33, 561–576.

Volkova, N.A., 1981. Arkitarkhi verkhnego dokembriya Yugo-Vostochnoy Sibiri (ust'kirbinskaya svita) (Upper Precambrian acritarchs of southeastern Siberia; the Ustkirbinsk Formation). Byulleten' Moskovskogo Obshchestva Ispytatelej Prirody, Otdel Geologicheskij 56, 66–75 in Russian.

Whittaker, S.G., Sami, T.T., Kyser, T.K., James, N.P., 1998. Petrogenesis of 1.9 Ga limestones and dolostones and their record of Paleoproterozoic environments. Precambrian Res. 90, 187–202.

Woods, K., Knoll, A.H., German, T., 1998. Xanthophyte algae from the Mesoproterozoic/Neoproterozoic transition: confirmation of evolutionary implications. Geol. Soc. Am. Abstr. Prog. 30, A-232.

Xiao, X., Knoll, A.H., Kaufman, A.J., Yin, L., Yun, Z., 1997. Neoproterozoic fossils in Mesoproterozoic rocks? Chemostratigraphic resolution of a biostratigraphic conundrum from the North China Platform. Precambrian Res. 84, 197–220.